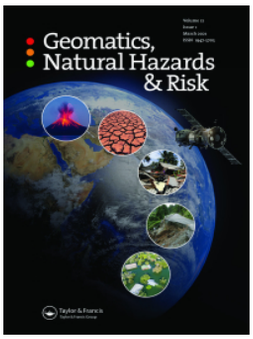

Geomatics, Natural Hazards and Risk

ISSN: 1947-5705 (Print) 1947-5713 (Online) Journal homepage: www.tandfonline.com/journals/tgnh20

Evaluating the impact of land use/land cover and rainfall changes on regional soil erosion

Wondifraw Nigussie , Husam Al-Najjar , Bahareh Kalantar, Worku Nega , Teshale Bizelk , K. V. Suryabhagavan & Niguse Adane

To cite this article: Wondifraw Nigussie , Husam Al-Najjar , Bahareh Kalantar, Worku Nega , Teshale Bizelk , K. V. Suryabhagavan & Niguse Adane (2025) Evaluating the impact of land use/land cover and rainfall changes on regional soil erosion, Geomatics, Natural Hazards and Risk, 16:1, 2520374, DOI: 10.1080/19475705.2025.2520374

To link to this article: https://doi.org/10.1080/19475705.2025.2520374

GEOMATICS, NATURAL HAZARDS AND RISK
2025, VOL. 16, NO. 1, 2520374
https://doi.org/10.1080/19475705.2025.2520374

Evaluating the impact of land use/land cover and rainfall changes on regional soil erosion

Wondifraw Nigussie[a], Husam Al-Najjar[b], Bahareh Kalantar[c], Worku Nega[d], Teshale Bizelk[e], K. V. Suryabhagavan[f] and Niguse Adane[d]

[a]Department of Land Administration and Surveying, Remote Sensing and Geo-informatics stream, Injibara University, Injibara, Ethiopia; [b]School of Computer Science, Faculty of Engineering and IT, University of Technology Sydney, Sydney, NSW, Australia; [c]RIKEN Center for Advanced Intelligence Project, Disaster Resilience Science Team, Tokyo, Japan; [d]Institute of Land Administration, Debre Markos University, Debre Markos, Ethiopia; [e]Department of Geography, Dilla University, Dilla, Ethiopia; [f]School of Earth Sciences, Addis Ababa University, Addis Ababa, Ethiopia

ABSTRACT

Climate change (CC), along with changes in land use and land cover (LULC), is among the primary forces driving soil erosion. Deforestation and anthropogenic activities have led to excessive soil erosion in the Ketar watershed. This study aimed to map the consequences of climate and LULC changes on soil erosion using soil loss equation factors integrated with Landsat imagery and geographic information systems. A maximum likelihood classifier was employed to categorize LULC classes, namely agricultural land, bareland, shrubland, forest, grassland, settlement, wetland, and waterbody. Rainfall data were derived from the Climate Hazards Group Infrared Precipitation with Stations (CHIRPS) dataset, and rainfall erosivity (R factor) was calculated for 1990–2020. The R factor, linked to rainfall intensity and amount, influences runoff and soil detachment. Cover management (C) and conservation practice (P) factors were derived from LULC and slope. LULC change significantly altered these factors. Results showed that between 2000 and 2020, cultivated land increased by 7.92%, while forest and wetland declined by 4.61%. The findings indicate that very high soil loss of 382.48 t $ha^{-1}yr^{-1}$, 368.8 t $ha^{-1}yr^{-1}$, and 412 t $ha^{-1}yr^{-1}$ occurred in 2000, 2010, and 2020, respectively. These findings support evidence-based watershed management, guiding sustainable land use planning and conservation interventions to protect livelihoods.

ARTICLE HISTORY
Received 19 November 2024
Accepted 5 June 2025

KEYWORDS
Climate change; environment; land use and land cover; RUSLE; soil loss

CONTACT Bahareh Kalantar bahareh.kalantar@riken.jp

Supplemental data for this article can be accessed online at https://doi.org/10.1080/19475705.2025.2520374.

1. Introduction

Soil erosion induced by water is defined as the loss of upper productive surface soil due to erosive precipitation and subsequent overflow (e.g. Ganasri and Ramesh 2016; Agegnehu et al. 2022). It is one of the most serious environmental degradations (e.g. Chalise et al. 2019; Bekele and Gemi 2021) and has become a significant issue for global sustainable development (Keesstra et al. 2018). This global environmental challenge primarily affects smallholder farmers (Gessesse et al. 2015). Soil erosion can be exacerbated by various natural and manmade factors (e.g. Alexandridis et al. 2015, Rust et al. 2022).

The rapid population growth has aggravated soil erosion and negatively impacted soil resources. There are many causes of soil erosion, such as land degradation, steep slope cultivation, and agricultural intensification (Haregeweyn et al. 2017; Nyssen et al. 2008). Additionally, Land use and Land cover (LULC) change has contributed to soil erosion. Several studies (e.g. Kavian et al. 2017; Gashaw et al. 2019; Girmay et al. 2020; Sime et al. 2020; Kulimushi et al. 2021) indicate a significant association between the severity of soil erosion and LULC change. At watershed, regional, and global levels, LULC change is a key source of soil loss (Kidane et al. 2019). The yearly average soil erosion varies substantially across different regional scales due to diverse LULC types and varying vegetation cover (Huang et al. 2020).

In the last century, significant LULC changes have occurred in Ethiopia, as they have in many other developing countries around the world. These changes were primarily driven by anthropogenic activities, such as deforestation, overgrazing, and unsustainable agricultural practices, which have accelerated soil erosion and led to soil nutrient deterioration (Eleni et al. 2013). LULC change also impacts landslide occurrence, which contributes to soil erosion and environmental degradation (Chen et al. 2019). In addition to LULC change, climate change (CC) has the potential to accelerate soil erosion (Huang et al. 2020). Due to land deterioration and poor farming practices in sloppy areas, Ethiopia's highlands are subject to soil erosion (Belayneh et al. 2019).

Ethiopia's highlands cover 43% of the country's land area and 95% of its cultivated land, and they are believed to have significant soil fertility potential (Desalegn et al. 2018). However, intensive farming methods, high rainfall erosivity and steep slopes exacerbate the problem of soil erosion (Nyssen et al., 2004; Fazzini et al. 2015; Haregeweyn et al. 2017; Nyssen et al. 2009). Rainfall is one of the most critical factors in CC-related soil erosion (Berberoglu et al. 2020; Borrelli et al. 2020; Ciampalini et al. 2020; Eekhout and De Vente 2020), influencing future trends in soil loss (Pal and Chakrabortty 2019). Thus, CC has impacted runoff and soil erosion in many watersheds by increasing precipitation concentration, volume, and intensity (Chen et al. 2019). This presents a key challenge for achieving regional sustainable development in the African Highlands, exacerbated by global CC and human activities (Li et al. 2021). Soil erosion negatively affects organic matter and topsoil, which are essential for plants development (Wijitkosum 2012). It significantly impacts food security, as evidenced by cases in developing countries (Eleni et al. 2013). Consequently, mapping and assessing soil erosion risk is an important tool for natural resource planning and management (Xavier et al. 2016).

Rain-fed agricultural areas in Ethiopia's highlands are expected to lose 940,893,165 tons of net soil per year, affecting two-thirds of the country's population (Hurni et al. 2015a; Hurni et al. 2015b). As a result, 50% of the highlands have been extensively degraded, leading to a 2.2% annual loss of land productivity (Greenland 2001). Consequently, considerable ecological deterioration has occurred, severely impacting the livelihoods of numerous households. In the central Main Ethiopian Rift (MER), the Ketar watershed is one of the areas with the highest rainfall erosivity and is heavily affected by soil erosion, according to Sime et al. (2020). They claim that heavy runoff during the summer makes agricultural land susceptible to erosion and flooding issues that impact communities living along the Ketar River's banks.

Soil erosion poses a significant environmental risk, but it can be mitigated through conservation measures (Kumar and Singh 2021). Researchers (e.g. Lee, 2004; Fu et al. 2005; Sotiropoulou et al. 2011; Haregeweyn et al. 2017; Lanorte et al. 2019; Girmay et al. 2020; Sidi Almouctar et al. 2021; Samela et al. 2022) have examined the valuation of soil erosion susceptibility or risk on regional and national scales using integrated empirical models like the Universal Soil Loss Equation (USLE) and the Revised Universal Soil Loss Equation (RUSLE) combined with geospatial techniques. These methods are crucial for providing improved evidence to implement soil and water conservation practices in eroded areas. Although these scientifically advanced models, tools, and studies exist, soil conservation practices in the Ethiopian Ketar watershed are not carried out due to a lack of scientifically measured, erosion-specific studies to prioritize hotspot areas that need protection.

A drawback of the RUSLE model (Gurmu et al. 2021; Sidi Almouctar et al. 2021) is that it ignores gully erosion. The RUSLE model is sensitive to uncertainties in input variables due to the nonlinear spatiotemporal variability of the parameters. Thus, the modeling outcomes should be validated using local measurement data (Wang et al. 2002). Validation and calibration of the RUSLE should involve soil erosion measurements from field plots, and it is advisable to conduct long-term soil loss experiments and measurements (Abu Hammad et al. 2004). While LULC alterations and CC are interconnected (Singh, 2023), the unique focus of this study is to assess how these two factors combine and affect soil erosion. Mainly, the C and P factors vary with changes in LULC, while the R factor varies with changes in rainfall. Therefore, the combined variations of these factors influence the extent of soil erosion across different decadal periods. This will provide policymakers with sufficient information about the site's LULC, climate, and soil loss status for future sustainable development. With these issues in mind, this study estimated potential soil loss using integrated RUSLE, Geographic Information System (GIS), and remote sensing techniques, considering rainfall and LULC changes over three decades (2000, 2010, and 2020). It also seeks to identify the current eroded hotspot areas to prioritize conservation measures in the Ketar watershed, Ethiopia.

2. Study area and data overview

2.1. Description of the study area

The Ketar watershed is located in the Arsi zone of Oromia region (Figure 1) which is part of the central MER. The study area is located within the Ziway-Shala basin, approximately 225 km from Addis Ababa. The watershed is bounded by latitudes 7° 21′ 42″–8° 8′ 5″ N and longitudes 38° 52′ 33″–39° 24′ 36″ E, with a total area of 3354 km^2. The Ketar River watershed region begins south of Mararo town, on the eastern Ethiopian plateau and flows towards its mouth at Lake Ziway, in the middle of the MER floor, west of Ogolcho town. The primary river within the watershed is Ketar.

2.2. Description of data and material

This research utilized various datasets and software to assess CC and LULC change, estimate potential soil loss, identify hotspot areas, and prioritize conservation measures. The analysis was conducted using software such as, ArcGIS 10.5, ERDAS Imagine version 2015, and Quantum GIS. Table 1 lists the main datasets used in this study.

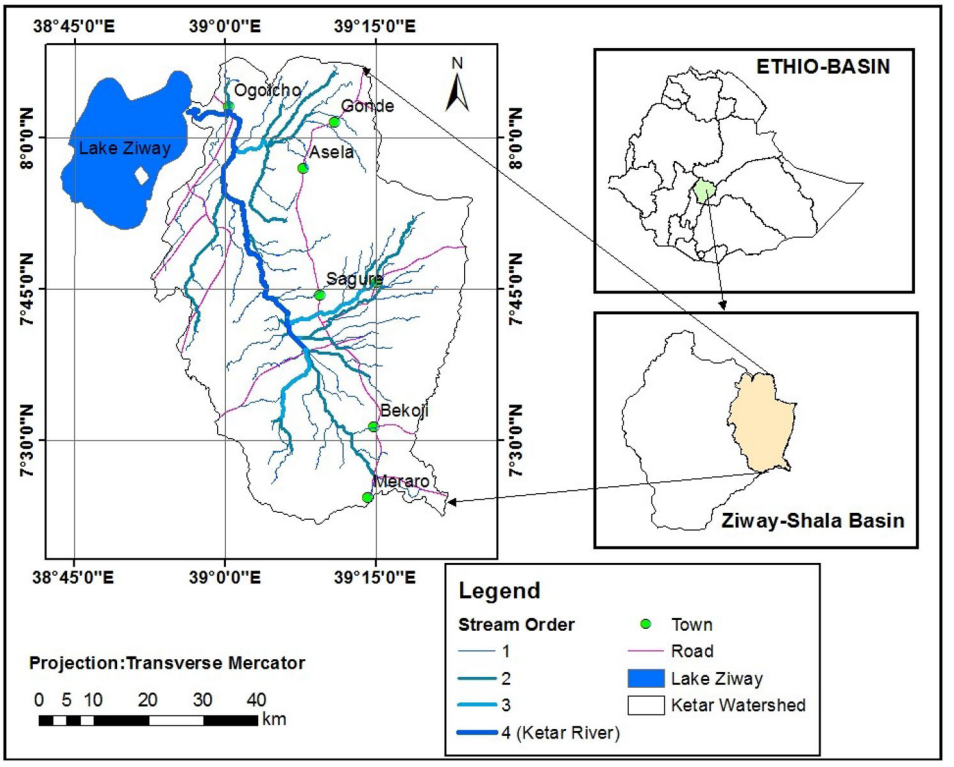

Figure 1. Location map of the study area.

Table 1. Geospatial data used.

Major Data	Resolution	Source	Purpose
Landsat Images (ETM+, and OLI)	30m	USGS	To generate LULC for 2000, 2010, and 2020 which was used to derive C and P factors over three decades
SRTM DEM	30m	USGS	To generate Slope length and steepness (LS-factor)
CHIRPS	5km (resampled to 30m)	EROS	To obtain rainfall erosivity (R factor) for 2000, 2010, and 2020
Soil	250m (resampled to 30m)	Ministry of Agriculture	To determine Soil erodibility (K factor)

Primary and secondary data from various sources were used in this analysis. Cloud-free Landsat imagery from the Operational Land Imager (OLI) and Enhanced Thematic Mapper plus (ETM+), covering path 168 and raw 055, was included as primary data. All imagery was obtained for free from the United States Geological Survey (USGS) website. Secondary data was sourced from records maintained by various organizations.

The Climate Hazards Group Infrared Precipitation with Stations (CHIRPS) dataset (https://www.chc.ucsb.edu/data/chirps) was developed in collaboration with scientists at the USGS Earth Resources Observation and Science (EROS) Center to provide reliable, up-to-date global data for applications such as trend analysis and seasonal drought monitoring (Ahmed et al., 2024). The CHIRPS satellite product was created by combining high-resolution climatology, field observations, and satellite imagery (Zhang et al. 2025). This quasi-global rainfall dataset estimates precipitation by blending real-time meteorological station data with infrared satellite observations at a 0.05° (5 km) resolution, providing continuous precipitation estimates from 1981 to the present. The performance of CHIRPS has been validated in multiple regions worldwide, using comparison with ground-based measurements and other satellite products. In particular, CHIRPS has been proven to be one of the most reliable satellite products in Africa, where sparse ground-based weather stations and data inconsistencies often hinder the performance of other satellite products (Du et al., 2024).

Recently, new observational resources, such as NASA and NOAA's gridded satellite-based precipitation estimates, have been used to create high-resolution (0.05°) precipitation climatologies. These refined climatologies minimize systematic bias in satellite-based precipitation data, which was a significant development in creating CHIRPS dataset (1981- present). The USAID Famine Early Warning Systems Network has also utilized CHIRPS for drought monitoring. The 'Africa' dataset offers a 0.10° grid resolution with a 6-hour time step (https://www.watres.com/CHIRPS/). Today, satellite rainfall products like CHIRPS are an alternative data source in areas with sparse rain gauge stations, as demonstrated by Paredes-Trejo et al. (2020), Ethiopia, for instance, has a limited rain gauge coverage. In East Africa, CHIRPS has been used for trend analysis and hydrological forecasting (Funk et al. 2015). For this study, monthly precipitation data from the CHIRPS data was used to calculate the long-term monthly averages over 30 years (1990–2020).

3. Methodology

Figure 2 shows the flowchart that visually outlines the various stages of data processing and analysis. It provides a step-by-step overview of the research process, from input data collection to soil loss estimation using the RUSLE model, and the identification of severely eroded areas to support better conservation measures. The flowchart highlights the key steps involved, including data acquisition, derivation of factors, and the calculation of the RUSLE model using R, K, LS, C, and P factors. In the three decades (2000, 2010, and 2020), the LULC change was assessed, and the C and P factors were derived. The rainfall distribution was analyzed (1990–2000, 2001–2010, and 2011–2020), and the R factor in the given period was determined. Each of these steps is essential for assessing soil erosion and its relationship with land cover and rainfall dynamics over the study period.

3.1. Image processing

The purpose of image processing is to reduce distortions and enhance the quality of the data (Ullah et al. 2024). Radiometric calibration and correction are essential image processing stages when comparing datasets across multiple periods to enhance the precision and interpretability of remote sensing data. Radiometric calibration is the way of transforming unprocessed sensor data (digital numbers) into physically meaningful units, such as converting Landsat digital numbers (DNs) to reflectance value; radiometric correction is the process of eliminating aberrations brought on by instrumental or environmental factors, such as fluctuation in the sun's angle, atmospheric

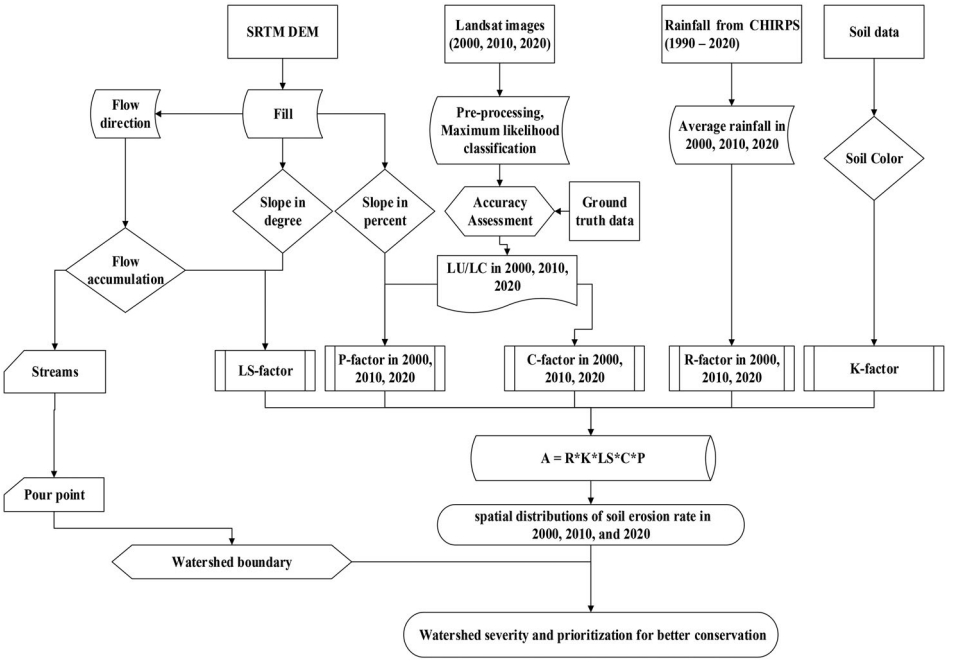

Figure 2. Overall methodology of the study.

interference, or sensor noise. The images were processed using the open-source, cost-free Quantum GIS (QGIS) software (Abdurahman et al. 2023). Atmospheric correction was performed using a Semi-Automatic Classification Plugin based on the Dark Object Subtraction (DOS) technique (Chavez, 1988), as recommended by Mohajane et al. (2018).

In this study, the DOS algorithm was applied to perform the atmospheric correction on the ETM+ images from 2000 and 2010, and on the OLI image from 2020. Each band of the ETM+ and OLI images, with a 30-metre resolution, was converted accordingly (Li et al., 2010); Abdurahman et al. 2023). Multi-temporal Landsat imageries from TM, ETM+, and OLI sensors are used to classify and predict LULC dynamics (Ullah, Ahmad, et al. 2025). For long-term LULC change studies, Landsat products offer remarkable advantages in scientific research because of their unique continuity (1972–present). For this study, Landsat ETM+ and OLI imagery were selected due to their uniform spatial resolution (30 m), temporal resolution (16 days), free accessibility, and wide spatial coverage.

3.2. LULC classification

The process of image interpretation and classification was used to extract the LULC information from multiband raster imageries (Li et al. 2014). Supervised classification using the maximum likelihood classifier has been widely applied due to its accessibility, and it doesn't need a lengthy training procedure (Currit 2005; Pal and Mather 2003; Nigussie et al. 2019; Osunmadewa et al. 2018; Abdurahman et al. 2023). When using the Maximum Likelihood Classifier for supervised classification, the analyst defines representative samples for each land cover category, achieving an effective classification with minimal cost and time, while ensuring the use of a significant amount of training data. Therefore, this study employs the standard Maximum Likelihood Classification technique, combining it with field verification and Google Earth imagery for accuracy assessment (Alam et al. 2020). LULC data in this research was derived from Landsat ETM+ and OLI images for 2000, 2010 and 2020. The classified LULC categories included farmland, bareland, grassland, forest, built up, wetland, shrubland, and waterbody. The Global Positioning System (GPS) data supported the post-classification process. After classifying the images into LULC classes, the accuracy assessment is an important procedure that checks how well the classified LULC map matches the real ground. Thus, field trips were conducted to improve LULC categorization and validate ambiguity. Given the potential for classification errors, an accuracy assessment of the output maps was conducted using established confusion matrix statistical techniques (Alam et al. 2020). Classification accuracy was estimated by calculating overall accuracy and the kappa coefficient (Sharma et al. 2018). In this study, all the raster layers' accuracies (2000, 2010, and 2020) were evaluated using an error-matrix. The classification for 2000 and 2010 were verified through local community discussions and Google Earth history, while the 2020 classification was assessed using field data and Google Earth references. Using those reference data, overall accuracy and the kappa coefficient were computed (see supplementary material). A classified LULC with an overall accuracy value of more

than 85% is acceptable (Girmay et al. 2021). The Kappa values lie between 0 and 1, with Kappa values >0.80 represent a strong agreement and good accuracy, between 0.40 and 0.80 indicate a middle accuracy, and <0.40 indicate a poor agreement between classification and observation (Barakat et al. 2018). The overall accuracy and kappa coefficient were computed based on Equation 1 and 2, respectively (Abdurahman et al. 2023).

$$Overall\ Accuracy = \frac{\sum_{i=1}^{r} x_{ii}}{\mathrm{N}}\ \mathrm{X}\ 100 \tag{1}$$

$$Kappa\ Coefficient = \frac{N\sum_{i=1}^{r} x_{ii} - \sum_{i=1}^{r}\left(x_{i+} * x_{+i}\right)}{\mathrm{N}^2 - \sum_{i=1}^{r}\left(x_{i+} * x_{+i}\right)} \tag{2}$$

where r is the number of rows in the matrix, x_{ii} expresses the total number of correctly classified pixels in row i and column i, N is the total reference data, x_{i+} and x_{+i} are the marginal totals of row i and column i.

3.3. Soil loss estimation (the RUSLE model)

Potential soil loss estimation has been carried out using a widely used and evaluated soil erosion model, originally developed as the USLE (Wischmeier and Smith 1978) and later modified into the RUSLE (Renard et al. 1997). The RUSLE is a popular model applied in various studies to assess rill and inter-rill soil erosion (e.g. Kulimushi et al. 2021). Hurni (1985) adapted it to the conditions of the Ethiopian highlands and calibrated most of the variables. The RUSLE model also effectively illustrates the connection between LULC change and soil erosion (e.g. Phinzi and Ngetar 2019). Given its, adaptability, usefulness in situations with limited data, and acceptance in Ethiopian highlands, RUSLE was chosen for this investigation.

The RUSLE model calculates soil erosion by factoring in climate, soil properties, topography, cover management, and conservation strategies. The equation for the RUSLE soil loss estimation model is expressed in Equation 3.

$$A = R \times K \times LS \times C \times P \tag{3}$$

where A is the estimated annual soil loss (t ha^{-1} $year^{-1}$), R is the rainfall erosivity factor (MJ mm ha^{-1} h^{-1} $year^{-1}$), K is the soil erodibility factor (t ha^{-1} MJ^{-1} mm^{-1}), LS is the slope length and steepness factor (dimensionless), C is the land use/cover factor (dimensionless) and P is the conservation support practice factor (dimensionless).

3.3.1. R-factor (rainfall erosivity) estimation

Ethiopian rainfall distribution has shown high variability across space and time due to complex topography (Reda et al. 2015); which is characterized by both seasonal and inter-annual spatial inconsistency (Alhamshry et al. 2019). The Ketar watershed is characterized by rugged topography, which ranges from 1628 to 4171 meters above mean sea level. The altitudinal variation in the Ketar watershed results in differing rainfall distribution, with highland areas receiving more rainfall, and lowland areas

receiving less. The amount, intensity, and distribution of rainfall govern the R factor (Amsalu and Mengaw, 2014). The R factor quantifies the erosive force of particular rainfall events (Gashaw et al. 2019). According to Renard et al. (1997), soil erosion is the reason for the R factor, which is the kinetic energy of rainfall storms. Hurni (1985) developed a regression empirical equation for the highlands of Ethiopia (Equation 4). In Ethiopia, where there was a lack of high-resolution rainfall intensity data, Hurni's work sought to localize the R-factor estimation. He conducted a statistical analysis of Ethiopian highland erosivity trends and rainfall data from metrological stations. Using restricted observed R values and matching them with corresponding annual rainfall, Hurni carried out regression analysis. The minimal threshold below which rainfall has no discernible effect on erosivity is considered by the intercept −8.12. The R rises with precipitation, as shown by the slope of 0.562. Several studies have applied Hurni's empirical erosion model to calculate the R factor and assess soil erosion in Ethiopia (e.g. Gelagay and Minale 2016; Zerihun et al. 2018; Heyder et al. 2023; Abro and Debie 2024; etc.). Therefore, due to a lack of data in the study site, we estimated the R factor by adopting Hurni's empirical equation.

$$R = -8.12 + 0.562P \tag{4}$$

where R is the rainfall erosivity factor (number) and P is the mean annual rainfall (mm). In this study, the R factor was calculated based on Hurni (1985) using CHIRPS data.

3.3.2. K-factor (erodibility) estimation

The K-factor expressed in t $ha^{-1} MJ^{-1} mm^{-1}$ characterizes the soils' vulnerability to erosion and reflects the intrinsic resistance of the soil to particle separation and transport by water erosion (Renard et al. 1997). Various soil properties, such as texture, structure, color, organic matter, and permeability, govern soil erodibility. The color of the soil reveals its composition of minerals, texture, and amount of nutrients, and those have an impact on erosion. For Ethiopian condition, Hurni (1985) developed a method for calculating the K factor based on soil color. This study identified the K factor of the research site based on soil color.

3.3.3. Topographic (LS factor) estimation

The gradient that influences flow velocity represents the local slope gradient (S-factor) (Renard et al. 1997), while the distance between the origin of overland flow to the point where deposition begins or flow is concentrated into rills in a defined channel represents the slope length (L-factor) (Wischmeier and Smith 1978). Topographic influence is considered a primary factor governing soil erosion (Farhan et al. 2013). On the steeper and longer slopes, erosion by water is greater due to the topography's increased runoff influence (Gashaw et al. 2019). Conversely, on gentle and shorter slopes, soil erosion by water is lower. Therefore, the LS factor is one of the main surface features of the model for erosion. The 30-meter resolution SRTM DEM was used directly to determine the S values. Similarly, flow accumulation derived from the DEM using fill and flow direction procedures. The LS factor was computed in

ArcGIS raster calculator using the map algebra expression in Equation (5) suggested by Mitasova and Mitas (1999); and Simms et al. (2003).

$$LS = \left(\frac{pow((\text{flow accumulation}) \times \text{cell size}}{22.13, 0.6}\right) \times \left(\frac{pow(\sin((slop) \times 0.01745}{0.0896, 1.3}\right) \quad (5)$$

3.3.4. Cover management (C factor) estimation

The C factor reflects how soil loss is influenced by land use, crop cover, and management strategies, rather than losses from bare fallow areas (Haregeweyn et al. 2017). It indicates the reduction in soil erosion brought on by ground cover and vegetation canopy. C values range from 0 for non-erodible conditions to 1 for more erodible conditions, often seen in extensive tillage situations, indicating varying levels of erodibility (Belay and Mengistu 2021). The normalized difference vegetation index (NDVI) and LULC classification maps are the most used techniques for estimating C-value. Hurni (1985) suggested C-values for forest land, shrub land, cultivated land, and grassland, while Moges and Bhat (2017) suggested C-values for bare ground and built-up area. Soil erosion is potentially more likely in areas without a developed vegetative layer because areas with less vegetation typically have higher C values (Ozsahin et al. 2018). Thus, there is less vegetation cover and more soil erosion when the C factor is larger. The C factor varies from 0 to 1 based on the LULC type (Gelagay and Minale, 2016; Tsai et al. 2021). This work independently derived the C-factor using the LULC data for 2000, 2010, and 2020 based on earlier research (e.g. Hurni, 1985; Gelagay and Minale, 2016; Moges and Bhat, 2017; Tsai et al. 2021).

3.3.5. Conservation practice (P factor) estimation

The term "P factor" describes how land conservation measures reduce the amount and speed of soil erosion and rainfall-runoff (Wischmeier and Smith 1978). According to Markose and Jayappa (2016), the conservation practice factor represents the ratio of soil erosion from land treated with a specific conservation measure to the corresponding soil loss from upslope and downslope tillage. Control measures that reduce runoff's potential for erosion are considered by the P factor, as they influence drainage patterns, runoff concentration, runoff velocity, and the hydraulic forces that runoff exerts on soil. The area with no management practices is given the highest score on the P factor, which ranges from 0 to 1. For this study, the P-factor was determined based on the slope present, and LULC of 2000, 2010 and 2020, with values ranges ranging from 0 to 1. The generated P-factor map is used to understand the conservation practices implemented in the study area. This factor considers control practices that reduce the erosive power of rainfall and runoffs by affecting drainage patterns, runoff concentration, and runoff velocity. The P-factor values were generated by classifying the land into farming and other major land use types. Since many management practices heavily rely on the area's slope, agricultural land (Table 2) was divided into six slope classes, with a P-value assigned to each class.

Table 2. P-Value for the study area (adapted from Wischmeier & Smith, 1978).

LULC	Slope (%)	P factor
Agricultural land (cultivated land)	0–5	0.1
	5–10	0.12
	10–20	0.14
	20–30	0.19
	30–50	0.25
	50–100	0.33
Other land	All	1.00

4. Results

4.1. Spatiotemporal classifications of LULC

The accuracy of the LULC maps, validated using ground truth data, was high for all three study years, indicating reliable classification results (see Supplementary material). Classified LULCs with overall accuracy of 85.97%, 87.98% and 88.14% were achieved, with kappa coefficient of 0.83, 0.85 and 0.86 for 2000, 2010, and 2020, respectively. Multi temporal raster layers were generated, and corresponding statistics were compared to estimation LULC changes. During 2000 (Figure 3a), agriculture was the main LULC type, accounting for 58.58% of the research site, followed by bareland (18.76%), grassland (9.66%), forest (7.52%), and Shrubland (4.71%) (Table 3). Waterbody, wetland, and built-up areas made up a small proportion of the landscape, at 0.07%, 0.33%, and 0.36%, respectively. Similarly, in 2010 (Figure 4a), agriculture increased and occupied the largest portion (62.10%) of the study landscape, followed by bareland (18.74%), forest (7.18%), and grassland (6.47%). Shrubland and settlement area covered 4.71%, and 0.49% of the total area, respectively. The remaining portions were occupied by waterbody and wetland, which covered 0.09% and 0.20%. In 2020, agriculture continued to be the dominant LULC type, with a proportion of 66.5%. In contrast, bareland decreased, covering 11.24%. Unlike the period from 2000 to 2010, grassland increased and covered 8.40% of the total study area. Shrubland showed an increase during the three study periods, covering 8.79% in 2020. Settlement areas and waterbody covered 0.85%, and 0.11% of the whole area, respectively, both showing an increase (Figure 5a) compared to previous years. Conversely, forest and wetland areas were degraded, covering 3.11% and 0.13%, respectively.

The change detection result revealed considerable changes in LULC during the last three decades (2000–2010–2020) across the study area. The details of LULC changes within the study area during the selected period are illustrated in Table 4, and 5. There was a continuous increase in the spatial extent of agriculture, shrubland, and settlement. In contrast, forest and wetland areas significantly decreased from 2000 to 2020. During the periods from 2000 to 2010 and from 2010 to 2020, 3167.5, and 2147.29 sq km, respectively (i.e. the sum of the diagonal elements), of the total landscape remained unchanged.

4.2. Cover Management (C) and Conservation Practice (P) Factors

The factor values for the research region ranged from 0 to 0.1 according to the analysis (C). A higher C value indicates that the designated LULC is highly susceptible

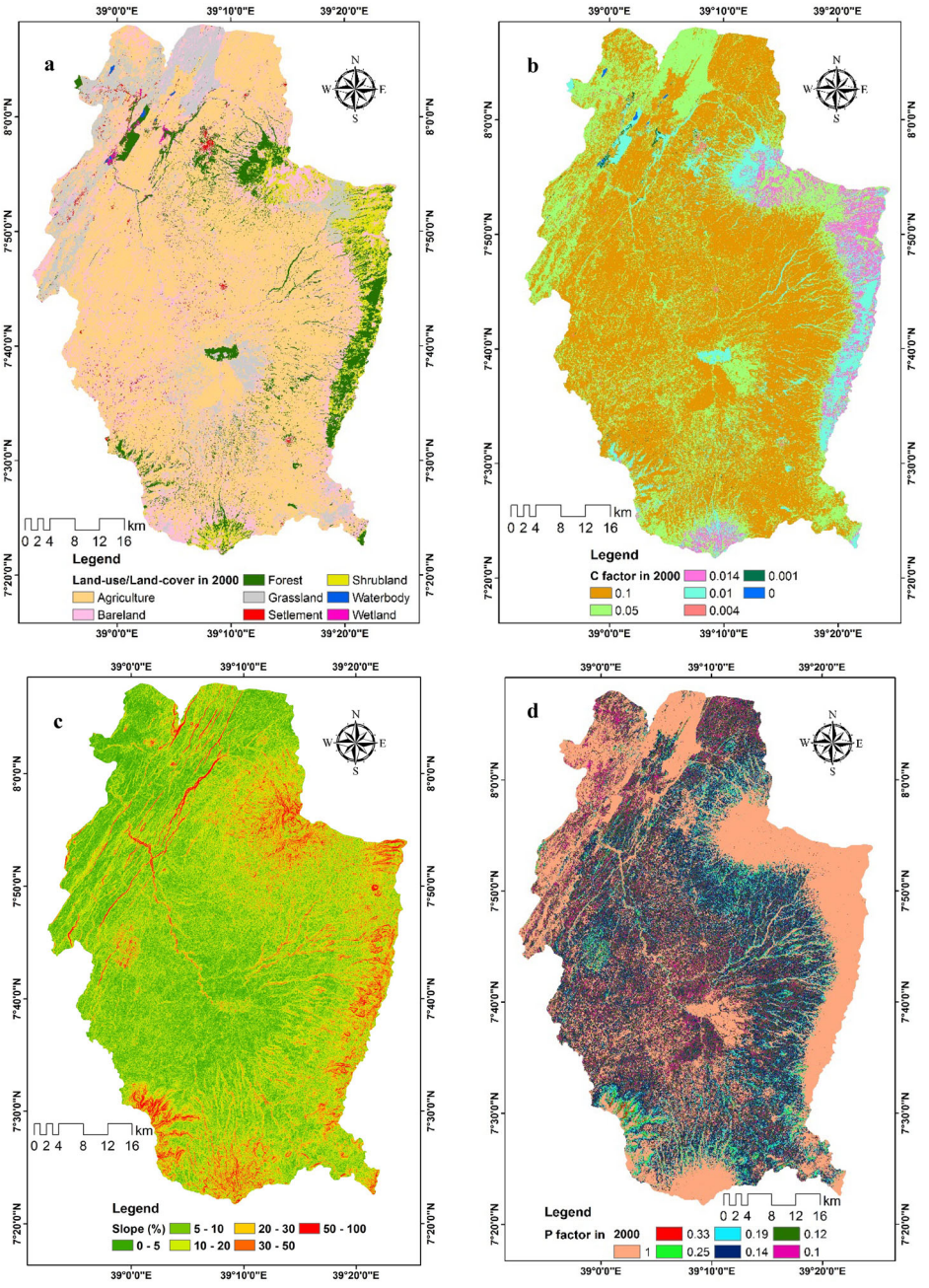

Figure 3. LULC in (a) 2000, (b) C factor, (c) slope (%),and (d) P factor.

to soil erosion, while a lower value indicates a less vulnerable land cover type in the study area. The C factor values associated with respective LULC type were (0, 0.001, 0.004, 0.01, 0.014, 0.05 and 0.1) in a waterbody, wetland, settlement, forest, shrubland, grassland, bareland and agriculture (Figure 3b, 4b, and 5b). Agricultural land has a higher C factor value than other LULC types because it is more susceptible to

Table 3. LULC areas for the reference years 2000, 2010, and 2020 in the study areas.

	2000		2010		2020	
LULC Types	Area (sq km)	%	Area (sq km)	%	Area (sq km)	%
Agriculture	1964.85	58.58	2082.71	62.10	2230.41	66.50
Bareland	629.13	18.76	628.59	18.74	407.15	11.24
Forest	252.14	7.52	240.93	7.18	104.23	3.11
Grassland	324.16	9.66	217.18	6.47	280.27	8.40
Settlement	12.12	0.36	16.59	0.49	28.74	0.85
Shrubland	158.07	4.71	158.08	4.71	294.96	8.79
Waterbody	2.57	0.07	3.05	0.09	3.75	0.11
Wetland	10.96	0.33	6.87	0.20	4.34	0.13
Total	3354	100	3354	100	3354	100

erosion. Due to degraded land cover and farming without conservative practices, the center portion of the north-south route has a high C-factor raster map value. Pasture and forest land had the lowest values in the northeast and southwest, which are the most central parts of the research area. The P-value (Figure 3d, 4c, and 5c) in agricultural land has increased as the slope percentage increased from 0 to 100% (Figure 3c), while all other LULC types contributed similar P-values.

4.3. Average annual rainfall and erosivity factor

In the Ketar watershed, the rainy season lasts from March to October, with June, July, and August receiving the most rainfall. The processed average annual satellite rainfall ranged from 651.5 to 1245.6 mm (1990-2000) (Figure 6a), 686.9 to 1183.88 mm (2001-2010) (Figure 7a), and 682.1 to 1256.2 mm (2011-2020) (Figure 8a). Notably, rainfall decreased from 2001 to 2010 compared to 1990 to 2000, while it increased during 2011 to 2020. In the majority of the research site, the distribution of rainfall was directly related to elevation (altitude). Over the three decades, the highest rainfall occurred in the eastern and south-western highlands. The R factor, measured in MJ mm ha^{-1} $h^{-1}yr^{-1}$ (Figure 6b, 7b, and 8b), for the three consecutive decades was derived from average annual rainfall and plays a major role in estimating soil erosion. Since the R factor is directly proportional to rainfall, the R-factor maps reveal very high values in the eastern highlands (Chilalo, and Galama mountains) and low values in the lowlands of the rift floor.

4.4. Soil erodibility (K factor)

The K-factor values of the Ketar watershed comprise five different colors of soil, corresponding to six soil classes. Chromic Luvisols and Haplic Luvisols (Brown or Redish brown), Mollic Andosols and Vitric Andosols (black), Eutric Cambisols (very dark gray), Eutric Fluvisols (yellow), Eutric Vertisols (very dark grayish brown), and Vertic Cambisols (brown) are the main soil classes in the research area (Table 6 and Figure 9a). The K-factor value, measured in t ha^{-1} MJ^{-1} mm^{-1}, was specifically allocated based on the color of each soil class (Table 6 and Figure 9b).

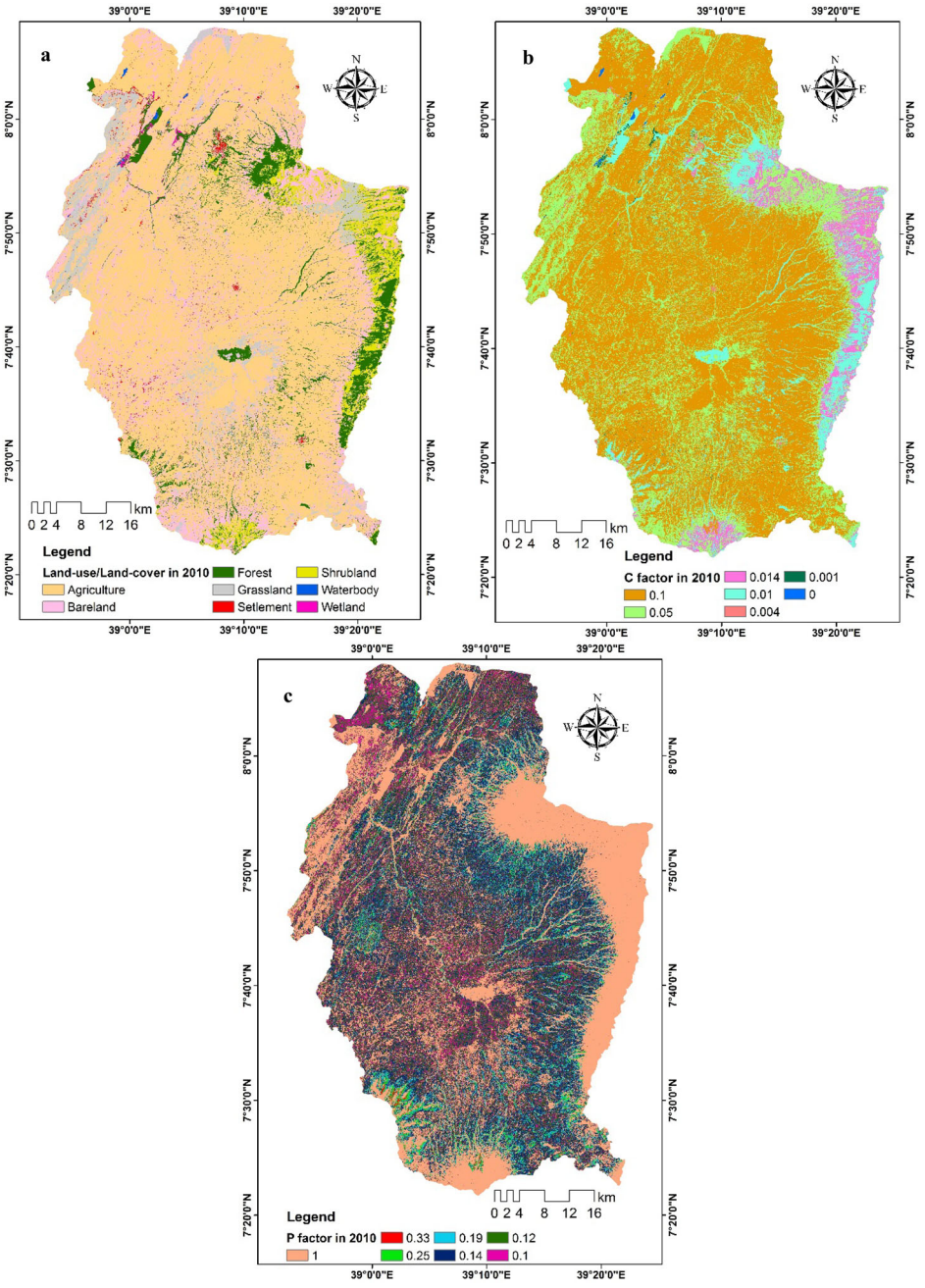

Figure 4. LULC in (a) 2010, (b) C factor, and (c) P factor.

4.5. Topographic (LS) factors

The LS factor in the current study ranges from 0 in the bottom portion of the watershed to 180.32 in the upper portion, which has the greatest slope. This suggests that the hills, mountainous areas (in the east and south), and lineament or faults (in the

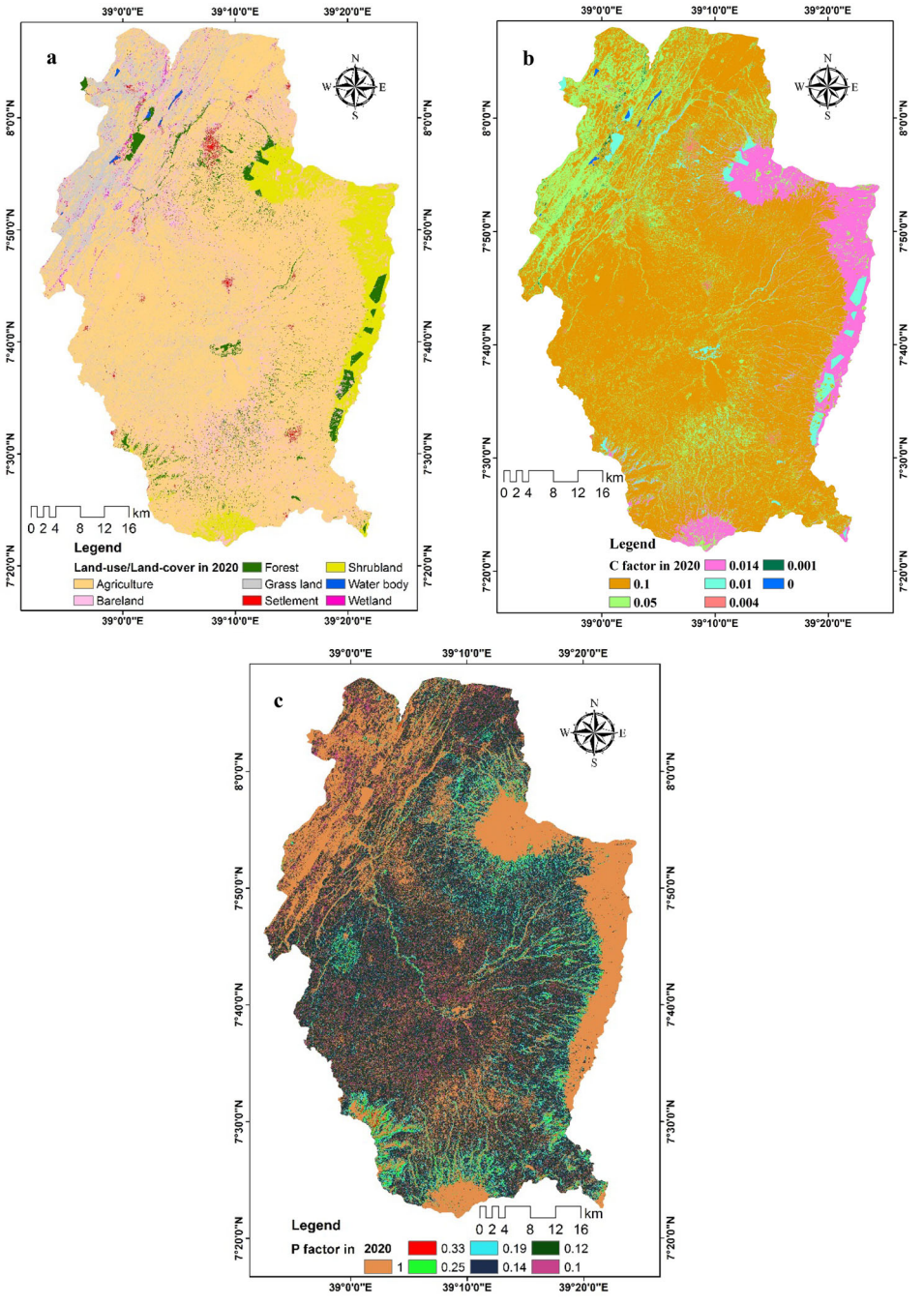

Figure 5. LULC in (a) 2020, (b) C factor, and (c) P factor.

northwest) of the watershed are significantly impacted by the combined slope length–steepness (LS) factor for soil loss (Figure 10). Conversely, in the lower and middle portions of the watershed, the topographic (slope length–steepness) component has a negligible impact on soil erosion.

Table 4. LULC change transition matrix (in sq km) from 2000 to 2010.

LULC	Agriculture	Bareland	Forest	Grassland	Settlement	Shrubland	Waterbody	Wetland	Total area in 2000
Agriculture	**1958.1**	0.21	0.01	4	2.4	0.01	0.11	0.01	**1964.85**
Bareland	0.77	**620.3**	0.03	7.8		0.23			**629.13**
Forest	2.87	0.08	**230.88**		0.03	18.28	0		**252.14**
Grassland	116.81	4.5	0.01	**199.38**	2.15		0.36	0.95	**324.16**
Settlement	0.11		0		**12.01**	0			**12.12**
Shrubland	0.01	3.5	10	5		**139.56**			**158.07**
Waterbody	0.01		0			0	**1.96**	0.6	**2.57**
Wetland	4.03			1			0.62	**5.31**	**10.96**
Total area in 2010	2082.71	628.59	240.93	217.18	16.59	158.08	3.05	6.87	**3354**

Table 5. LULC change transition matrix (in sq km) from 2010 to 2020.

LULC	Agriculture	Bareland	Forest	Grassland	Settlement	Shrubland	Waterbody	Wetland	Total area in 2010
Agriculture	**1674.67**	188.95	5.93	189.12	8.81	14.1	0.65	0.48	**2082.71**
Bareland	370.15	**160.97**	1.56	20.96	2.9	72.05	0	0	**628.59**
Forest	46.43	19.92	**96.08**	1.35	1.89	75.26	0	0	**240.93**
Grassland	122.56	21.45	0.17	**66.69**	0.26	5.02	0.03	1	**217.18**
Settlement	1.64	0.06	0	0.38	**14.5**	0.01	0	0	**16.59**
Shrubland	13.19	15.76	0.41	0.08	0.14	**128.49**		0.01	**158.08**
Waterbody	0.09	0.04	0	0.03			**2.89**		**3.05**
Wetland	1.68		0.08	1.66	0.24	0.03	0.18	**3**	**6.87**
Total area in 2020	2230.41	407.15	104.23	280.27	28.74	294.96	3.75	4.49	**3354**

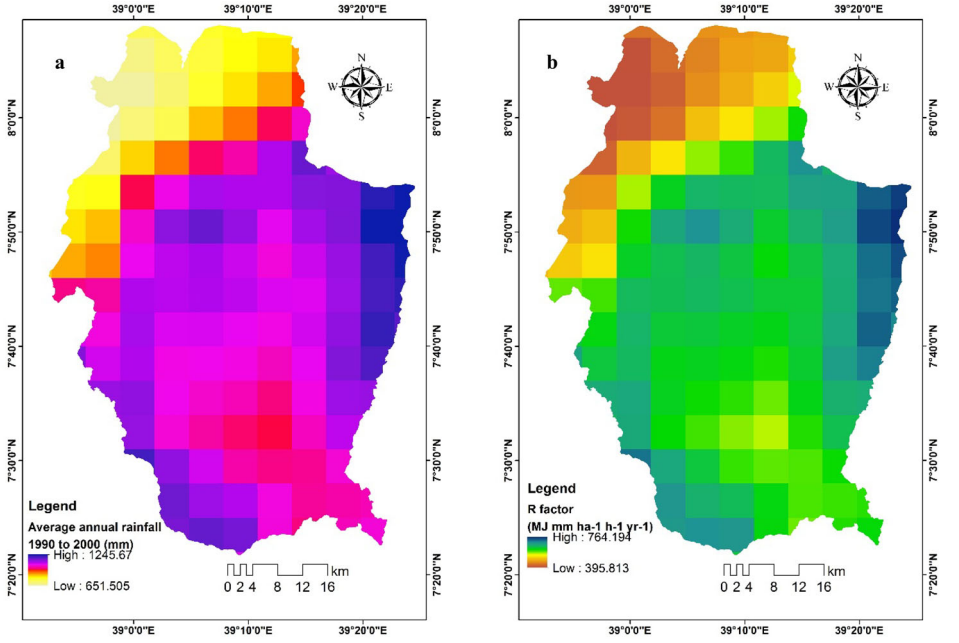

Figure 6. Average annual rainfall from (a) 1990 to 2000, (b) R factor.

4.6. Potential annual soil loss

The final map showing the potential annual soil loss of the watershed was produced by overlaying and multiplying the five parameters (K, R, LS, C, and P). Each layer

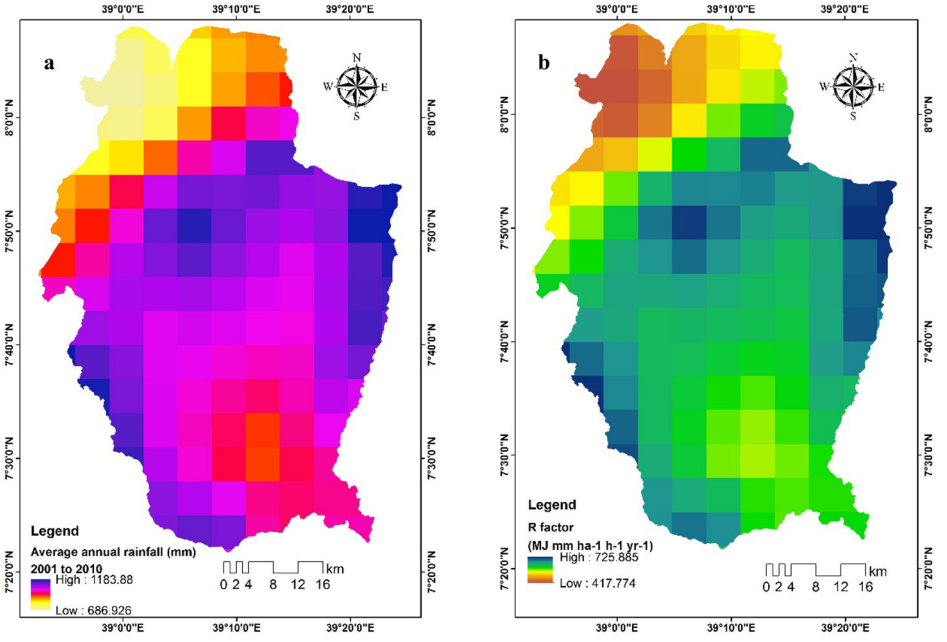

Figure 7. Average annual rainfall from (a) 2001 to 2010, (b) R factor.

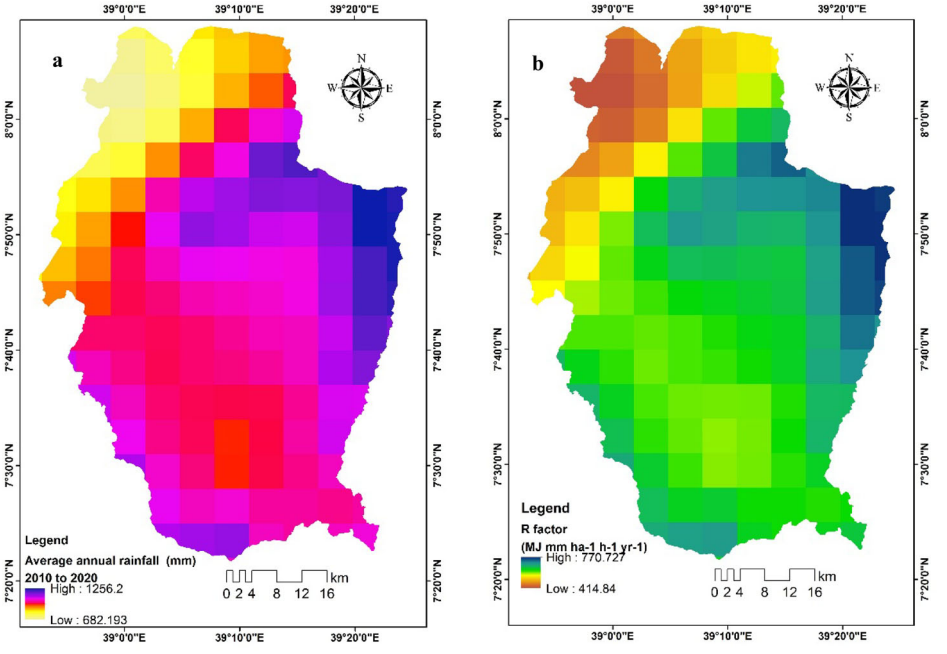

Figure 8. Average annual rainfall from (a) 2010 to 2020, (b) R factor.

was organized with a resampled cell size (30 * 30 m). Additionally, a statistical technique was utilized to categorize the soil loss risk levels in the study watershed and estimate the potential quantity of soil loss. The soil erosion map of the watershed was divided into five groups of administrative prioritization (Table 7 and Figure 11).

Table 6. Soil type, color, K-factor, and area coverage.

Soil type	Soil color	K factor (t ha^{-1} MJ^{-1} mm^{-1})	Area (sq km)	Area (%)
Chromic Luvisols	Brown (Redish brown)	0.2	517.6	15.43
Eutric Cambisols	Very dark gray	0.2	6.96	0.21
Eutric Fluvisols	Yellow	0.3	0.67	0.02
Eutric Vertisols	Very dark grayish brown	0.15	1604.89	47.85
Haplic Luvisols	Brown (Redish brown)	0.20	557.7	16.62
Mollic Andosols	Black	0.15	505.04	15.06
Vertic Cambisols	Brown	0.20	110.5	3.3
Vitric Andosols	Black	0.15	50.64	1.51

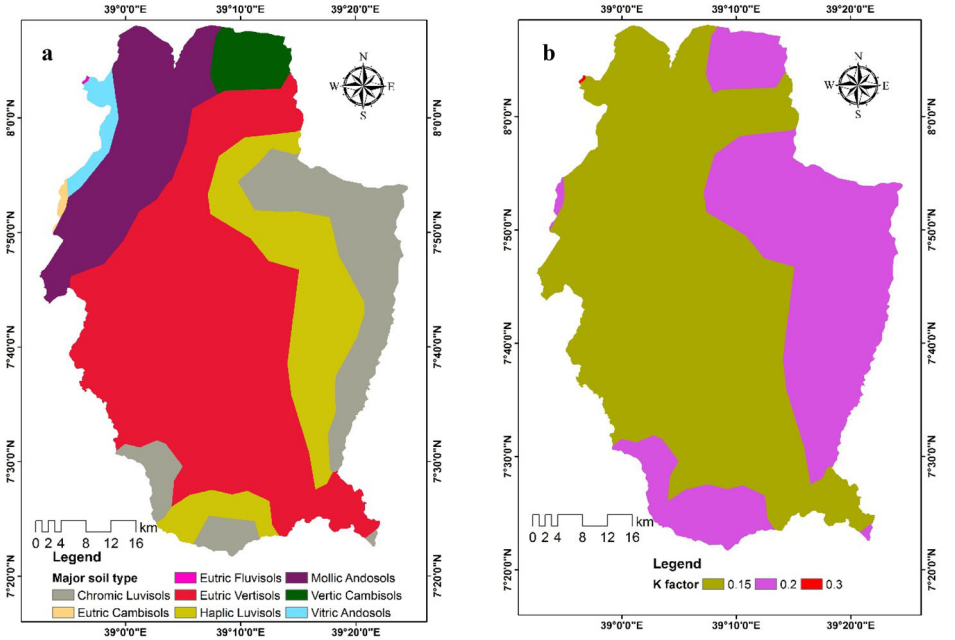

Figure 9. (a) Major soil type and (b) K factor of the study area.

In 2000, the estimated potential soil loss ranged from 0 to 382.48 t ha^{-1}year^{-1} (Figure 11a). This soil loss decreased to 368.8 t ha^{-1}year^{-1} in 2010 due to reduced rainfall (Figure 11b). However, in 2020, the potential soil loss increased to 412 t ha^{-1}yr^{-1} due to the combined effects of LULC change and CC (Figure 11c).

4.7. Identified severity areas needing urgent conservation measures

Highly eroded areas (severity classes) in 2020 were found in the eastern and southern parts of the steep mountainous regions. These are mostly located at altitudes ranging from 3200 – 4213 meters above sea level. A severely eroded area in the northwest (1600 – 2300 meters above mean sea level) is situated around faults, and lineaments (Wonji fault). Therefore, these areas (marked in red on the map) require urgent conservation measures (Figure 12). Some sample field photos (Figure 13) were taken at Kolicha Kebele, a site that needs conservation efforts and is near Chilalo Mountain. During field verification, seventy-nine ground truth points (Table 8) at eroded hotspot areas were collected and overlaid on the map of identified severity areas.

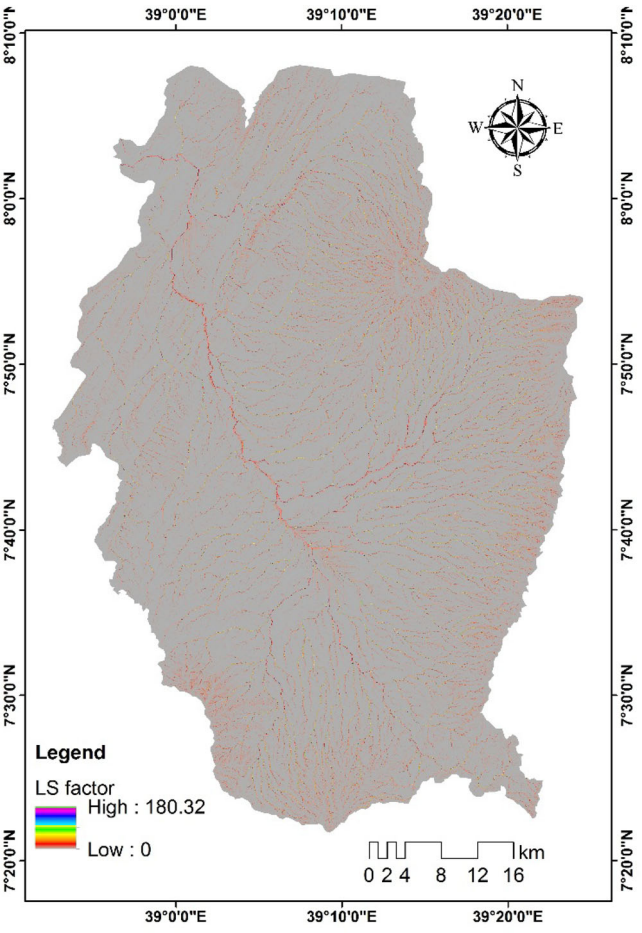

Figure 10. Topographic (LS) factor of the study area.

Table 7. Soil erosion severity classes and area coverage in each year.

	2000		2010		2020	
Soil erosion severity classes (t ha-1 year-1)	Area (ha)	Area (%)	Area (ha)	Area (%)	Area (ha)	Area (%)
Very slight (0–5)	169444.1	50.5	177218.3	52.8	167246.5	49.9
Slight (5–15)	101727.2	30.3	96782.3	28.9	97599.2	29.1
Moderate (15–30)	39715	11.8	37918.2	11.3	44138.6	13.2
Severe (30–50)	14900.7	4.4	14513.6	4.3	16250.7	4.8
Very severe (>50)	9613	3	8967.6	2.7	10165	3.03
Total	335400	100	335400	100	335400	100

The collected hotspot locational data coincided exactly with the severity areas, indicating that the identified potential annual soil loss by the RUSLE model was spatially correlated with the actual ground conditions.

5. Discussion

LULC change affects soil erosion, along with other influences such as climate, soil properties, and topography (Negese 2021). Changes in LULC are accelerating land

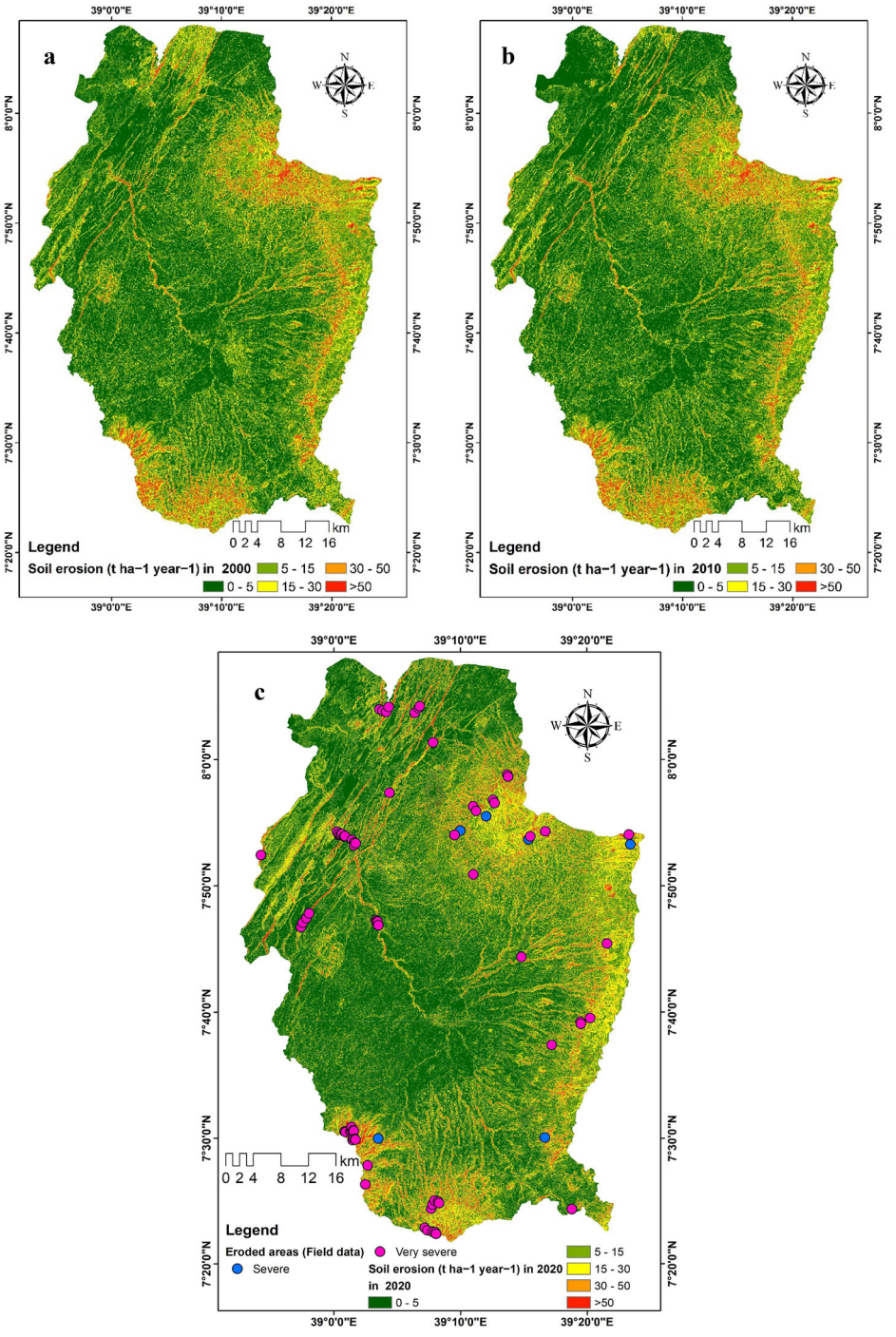

Figure 11. Estimated potential annual soil loss map in (a) 2000, (b) 2010, and (c) 2020.

degradation due to climatic and geomorphological factors in the area (Sharma et al. 2011). One of the under-researched issues in developing countries is measuring soil erosion, sediment output, and the sediment retention capacity of watersheds (Degife

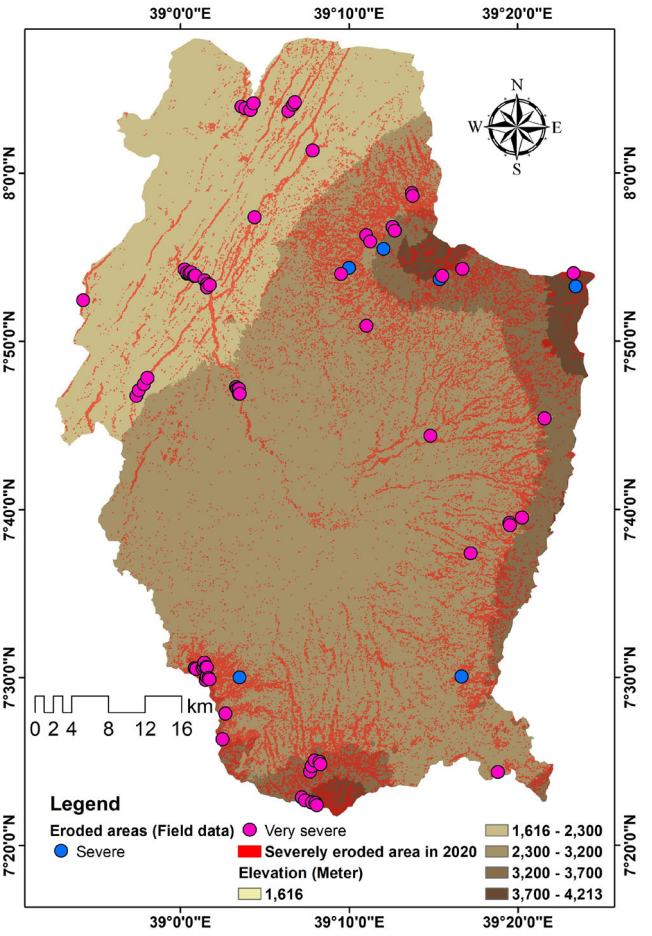

Figure 12. Identified severity areas that needs an urgent conservation measure.

et al., 2021). With rugged topography and high soil erosion, the Ketar watershed in Ethiopia is encircled by tall mountains (Chilalo and Galama), which rise 4176 meters above mean sea level. Most high mountain areas are sensitive to CC, and shifting climatic conditions may increase the risk of soil loss and land degradation (Wang et al. 2017). Consequently, increased rainfall leads to a rise in the annual R factor, which accelerates soil erosion (Belay and Mengistu 2021). Resampling of CHIRPS data has been conducted in previous studies such as Li et al. (2021) and Tesfamariam et al. (2022). In the current study, the CHIRPS product monthly rainfall was used to calculate annual maximum and minimum rainfall from 1991 to 2020 (Figure 14). The average maximum rainfall was 1245.6 mm (1990-2000), 1183.88 mm (2001-2010), and 1256.2 mm (2011-2020). The increasing annual maximum rainfall from 2010 to 2020 indicates that rainfall events became more intense, with a sharp rise observed. Additionally, the minimum annual rainfall also showed a slight increase. During this period, the study area experienced more frequent and intense rainfall events, which accelerated soil erosion. Over the three decades, high rainfall was observed in mountain areas, similar to findings by Nigussie et al. (2019). The R factor in these three

Figure 13. Field photographs of eroded soil areas at kolicha kebele.

consecutive decades was 764.194, 725.885, and 770.727 MJ mm ha^{-1} h^{-1} yr^{-1} respectively (Figure 15). In all periods, the highest R factors were recorded in the northeastern mountainous areas, which have a major impact on soil erosion. In a highly populated area, anthropogenic activities (such as agricultural practices without soil and water conservation measures, overgrazing, and deforestation) that induce land cover change are primarily responsible for CC and severe soil erosion (Pal et al. 2021). Areas with poor soil management (i.e. lacking conservation practices) are more prone to increased soil erosion, whereas non-intensive agricultural practices may reduce the rate of erosion. Recent research indicates that LULC and CC may significantly affect the severity of soil erosion at different spatiotemporal scales (e.g. Aneseyee et al. 2020; Berihun et al. 2019; Chakrabortty et al. 2020b; Ebabu et al. 2019; Luetzenburg et al. 2020; Tadesse et al. 2017; Taye et al. 2018). The conservation

Table 8. Ground truth data at eroded hotspot locations.

ID	X-Coordinate	Y-Coordinate	ID	X-Coordinate	Y-Coordinate
1	39.021641	7.508924	40	38.963702	7.790765
2	39.015321	7.508279	41	38.967015	7.797073
3	39.014092	7.508951	42	39.138237	7.41391
4	39.023163	7.510212	43	39.1372	7.416159
5	39.02601	7.509682	44	39.132389	7.417551
6	39.025338	7.51033	45	39.129504	7.412041
7	39.024593	7.497522	46	39.127953	7.406607
8	39.025684	7.500357	47	39.209645	7.946806
9	39.02826	7.498135	48	39.211646	7.943102
10	39.027601	7.499306	49	39.130517	8.022822
11	39.023295	7.514573	50	39.228772	7.98045
12	39.058126	7.499776	51	39.229635	7.9775
13	39.044348	7.464086	52	39.073115	7.956459
14	39.04143	7.438775	53	39.277663	7.500876
15	39.119732	7.380969	54	39.313323	7.405974
16	39.122911	7.377756	55	39.18364	7.938606
17	39.129662	7.375948	56	39.187555	7.932326
18	39.133099	7.375395	57	39.200669	7.924998
19	39.134418	7.372989	58	39.166549	7.906188
20	39.014462	7.898729	59	39.158775	7.900263
21	39.010273	7.901751	60	39.183785	7.848536
22	39.0041	7.904694	61	39.325492	7.651074
23	39.006415	7.901861	62	39.325047	7.653597
24	39.006348	7.900367	63	39.337525	7.658725
25	39.008726	7.900653	64	39.247124	7.73962
26	39.013211	7.89829	65	39.28684	7.623211
27	39.023744	7.893814	66	39.057697	7.786152
28	39.026418	7.88688	67	39.05745	7.786553
29	39.026349	7.890175	68	39.054933	7.787981
30	39.028592	7.889334	69	39.055838	7.786143
31	39.060032	8.066375	70	39.057448	7.782407
32	39.064128	8.064708	71	39.058444	7.781307
33	39.069014	8.063099	72	39.057691	7.781316
34	39.071988	8.069662	73	39.388797	7.900824
35	39.106513	8.061923	74	39.390813	7.887727
36	39.111355	8.06816	75	39.359892	7.756823
37	39.112982	8.070682	76	39.256368	7.894927
38	38.956256	7.779032	77	39.25871	7.898379
39	38.958723	7.784511	78	39.278724	7.905047
			79	38.903653	7.873919

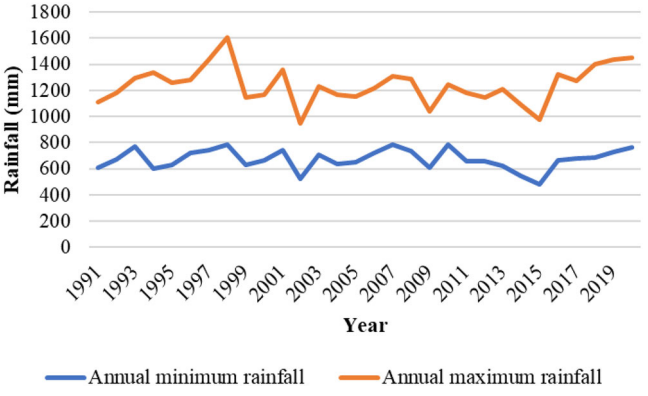

Figure 14. Annual maximum and minimum rainfall from 1991 to 2020.

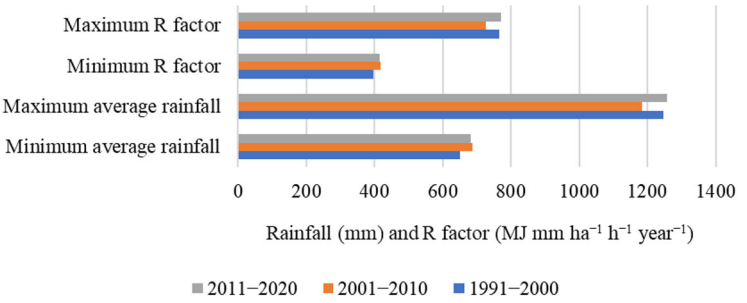

Figure 15. Decadal average minimum and maximum rainfall, and R factor.

of natural plant cover to cultivated land and general LULC dynamics are two prominent human-induced issues that have significantly contributed to the rise in soil erosion rates in Ethiopia (Negese 2021). Negese (2021) claims that the expansion of cultivated land at the expense of forest, shrubland, and grassland has increased Ethiopia's mean rate of soil erosion over the past forty years.

One of the main benefits of the RUSLE model is its adaptability to different geo-environmental and socioeconomic contexts (Duarte et al. 2021). This research used the RUSLE model to calculate annual soil loss over three decades. By overlaying and multiplying the five factors (C, P, R, K, and LS), the mean annual soil loss in the Ketar watershed was estimated at 0 to 382.48 t $ha^{-1}yr^{-1}$ in 2000, 0 to 368.8 t $ha^{-1}yr^{-1}$ in 2010, and 0 to 412 t $ha^{-1}yr^{-1}$ in 2020. CC is anticipated to affect soil erosion due to its impact on rainfall intensity (Maliqi and Singh, 2019). In this study, the decreased rate of soil erosion in 2010 was attributed to the reduced R factor compared to other years. These results align with Li et al. (2021), concluding that the impact of CC on soil erosion is greater than human influence. Due to the observed decline in rainfall between 2001 and 2010, we conducted a comparative analysis by applying the R-factor derived from the 2001–2010 rainfall data to estimate soil loss across the three decades. Using the actual R-factor from 1991 to 2000 rainfall, the estimated soil loss was 382.48 t $ha^{-1}yr^{-1}$. However, when the 2010 R-factor was applied, it decreased to 362.7 t $ha^{-1}yr^{-1}$. In 2020, the increased rainfall resulted in an estimated soil loss of 412 t $ha^{-1}yr^{-1}$. Nevertheless, when the R-factor from the second decade of rainfall was applied, the soil loss decreased to 396.9 t $ha^{-1}yr^{-1}$. This demonstrates that variations in the amount and intensity of rainfall influenced the R-factor, thereby affecting soil erosion. Here, we observed that even when the same amount of rainfall was applied across the study periods, the extent of soil loss increased (Figure 16) by 9.4% from 2000 to 2020, primarily due to changes in LULC.

During the specified periods, very severe soil loss was predominantly observed in agriculture areas, which encompass 1483.5 ha in 2000, 1586.7 ha in 2010, and 3648.5 ha in 2020 (Table 9). This increase can be attributed to heavy rainfall during the wet season, with most crops (such as teff, maize and barley) being planted at the start of the rainy period, resulting in significant soil erosion on relatively bare ground. This is consistent with the finding by Wang et al. (2018). As shown in Table 9, bareland, grassland, and shrubland areas contributed to severe soil loss. In contrast,

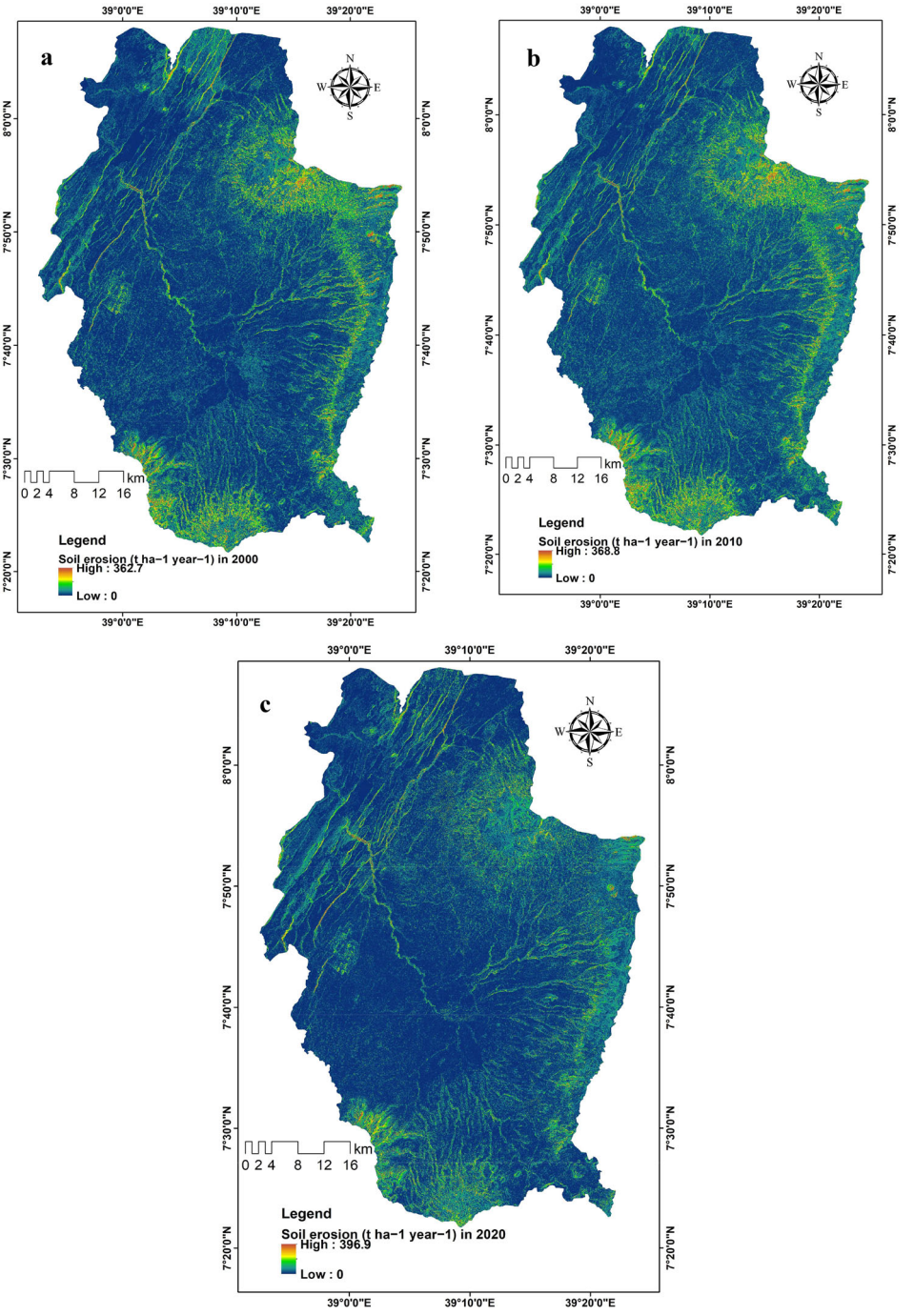

Figure 16. Estimated soil loss in 2000 (a), 2010 (b), and 2020 (c) using similar rainfall from 2001 to 2010.

waterbodies, and wetlands had less impact on soil erosion. However, wetlands experienced some severe soil erosion in 2020 due to degradation. Zhang et al. (2025) examined land use dynamics and urban expansion over four decades (1990–2030) and

Table 9. The area coverage of each LULC type in each severity class from 2000 to 2020.

Severity Class	Very slight (ha)			Slight (ha)			Moderate (ha)			Severe (ha)			Very severe (ha)		
Year	2000	2010	2020	2000	2010	2020	2000	2010	2020	2000	2010	2020	2000	2010	2020
Agriculture	131128	141920	137796	49045.7	49639	60704.4	12400.3	12550.6	17337.3	3849.8	3906	7385	1483.5	1586.7	3648.5
Bareland	14565.1	14938.6	8573.8	18509.4	18415	9485.8	13702.2	13879	7912.2	8245.3	8255.8	4635	6678.5	6112.4	4061.4
Forest	9916	9464.4	4077.5	11319.1	10987	3952.4	3554.9	2984.2	1650	356	340	262	284.8	288	330.1
Grassland	9091.3	5698.2	11184.5	14625	8784.4	11006	6027.5	4334	5732	1839.3	1455.8	1586	770	538.7	706.7
Settlement	1584	1589	1168.1	197.7	192	154.2	96.6	93.98385	107.3	21.3	24.7	58.2	7.8	7.5	45.7
Shrubland	1851.1	2199.4	2991.6	7755.7	8493.2	12054	4006.9	4054.2	11202	624.9	600	2230.1	457.4	432.5	928.5
Waterbody	190.3	190.2	352.6	3.7	3.7	3	1.7	1.5	3.1	0.3	0.5	0.7	0.1	0.04	1.6
Wetland	905.1	902	1051.3	53.8	55	208.7	14.9	15.7	179.8	3.9	4.6	87	1.1	1.1	58.9

recorded the progressive increase in the conversion of grassland and shrubland to urban areas. In this study the increased rate of built up areas were due to the conversion of grassland and agricultural land to settlement areas, which contributed to severe erosion in 2020. Due to unplanned urbanization, settlements were continuously increased, and vegetation decreased (Ullah, Khan, et al. 2025), which may increase soil erosion. Land use dynamics, such as the clearing of forests for agricultural expansion, are key factors escalating the severity of soil erosion (Kulimushi et al. 2021). According to Ullah, Ahmad, et al. (2025), agricultural lands increased steadily between 1990 and 2020. In the current study, agricultural land showed an increase mainly due to the conversion of forest, shrub, and grassland. Comparable to our work, Besha et al. (2024) investigated LULC dynamics in Ethiopia's Central Rift Valley and revealed a steady increase in areas of agriculture, built-up, and bareland while forests and grassland declined. In forest areas, there were moderate to severe soil losses observed, although they were not the primary driving factor. This was due to most forested areas being located in mountainous and sloped regions characterized by high rainfall. Land use and management techniques significantly impact soil loss (Rawat and Singh 2018). The C-factor, which fluctuated as LULC changed over time and space while the other components remained constant, was identified as the cause of spatiotemporal variation in soil erosion (Balabathina et al., 2019). In this study, the changes in soil loss across different classes and years were attributed to variations in the C-factor corresponding to changes in LULC. Due to LULC dynamics occurring between 2000 and 2020, the predicted average soil loss increased. This demonstrates that LULC has a substantial effect on soil erosion caused by water. High slope length and gradient values in the watershed contribute to the high soil erosion rate (Girmay et al. 2020; Kumar and Singh 2021). Similar to Girmay et al. (2020), the highest soil erosion rates over the three decades were observed at high LS values. For instance, in the northern part near the Ketar River, LS values greater than 100 result in soil loss exceeding 240 t $ha^{-1}yr^{-1}$. Therefore, in regions with high rates of erosion, it is imperative to immediately apply soil conservation strategies, as this study has identified. Fruit tree plantations, agroforestry, and terracing systems are examples of integrated techniques that should be given priority in order to guarantee the sustainable management of steep mountain regions of the current study site that are prone to erosion. Furthermore, to reduce soil loss in the heavily eroded portion of the research region, nature-based strategies such as integrating plants with engineering structures are advised. These methods not only lessen soil loss but also increase land production and adaptability to upcoming environmental changes.

This study's limitation is that, while the output was spatially validated by ground truth data, it was not possible to measure soil loss directly through the use of sediment traps in the field or through the creation of testing plots with recognized LULC types. Thus, we recommend that future studies should validate the model's output by direct soil loss measurements from the field. Further research should consider predicting the future LULC and CC. Additionally, studies should work to predict the soil loss trend, especially if no conservation measures take place in the current severely eroded hotspot areas.

6. Conclusions

This study assessed the combined impact of LULC change and rainfall variability on soil erosion dynamics in the Ketar watershed over three decades (2000–2020). The RUSLE model and geospatial techniques were used to map the extent of soil loss. The findings showed that forests, wetlands, and grasslands were lost in favor of a significant increase in agricultural land and settlements, which heightened the risk of soil erosion. Wetland degradation and the reduction in forest cover from 7.52% in 2000 to 3.11% in 2020 led to an expansion of areas susceptible to erosion. Although shrubland showed some recovery between 2010 and 2020, the detrimental effects of deforestation and agricultural expansion could not be offset by its growth. Climate variability also influenced soil erosion across the three decades. The variation in rainfall trends demonstrated how fluctuations in rainfall intensity and frequency impacted soil erosion. The worst soil loss, 412 t $ha^{-1} yr^{-1}$, occurred in 2020, underscoring the role that increased rainfall and ongoing land degradation play in increasing soil erosion. To better understand the effect of rainfall and LULC change on soil erosion, this study applied similar rainfall amounts across the three decades and observed an increase in soil loss extent, which was primarily attributed to changes in LULC. The results highlight how urgently appropriate land management techniques are needed to reduce soil loss, especially in areas that have been cleared for agriculture and deforestation. In areas significantly affected by erosion, the findings of this study can assist in implementing effective erosion management techniques. The local community should be made aware of the impact of LULC change on soil erosion, and it is advisable to practice Soil and Water Bioengineering (SWBE) conservation measures, along with other conservation and agricultural practices (Vianney Nsabiyumva et al. 2023). Fruit tree planting should be considered in places that are prone to erosion because it serves to reduce erosion and increases soil fertility by enriching the soil with organic matter. This study also recommends that planners and researchers consider the climate's impact on soil erosion and prepare accordingly. Future research should incorporate projections of both LULC and CC impacts on future soil loss extent.

Acknowledgments

The authors would like to acknowledge both the United States Geological Survey (USGS) and Earth Resources Observation and Science (EROS) Center for providing access to Landsat images and Climate Hazards Group InfraRed Precipitation with Station (CHIRPS) data free of charge in their data hub. We are also thankful to the RIKEN Centre for Advanced Intelligence Project (AIP), Tokyo, Japan for their support with the Article Processing Charge (APC).

Author contributions

CRediT: **Wondifraw Nigussie**: Conceptualization, Formal analysis, Methodology, Validation, Writing – original draft; **Husam Al-Najjar**: Investigation, Supervision, Visualization, Writing – review & editing; **Bahareh Kalantar**: Funding acquisition, Resources, Validation, Visualization, Writing – review & editing; **Worku Nega**: Project administration, Resources, Software, Writing – review & editing; **Teshale Bizelk**: Project administration, Writing – review &

editing; **K. V. Suryabhagavan**: Project administration, Writing – review & editing; **Niguse Adane**: Project administration, Writing – review & editing.

Ethics approval and consent to participate

There are no elements of the study that are concerned with using human or animal subjects in the lab.

Disclosure statement

No potential conflict of interest was reported by the author(s).

ORCID

Bahareh Kalantar http://orcid.org/0000-0002-2822-3463

Data availability statement

Data will be made available on reasonable request.

References

Abdurahman A, Yirsaw E, Nigussie W, Hundera K. 2023. Past and future land-use/land-cover change trends and its potential drivers in Koore's agricultural landscape, Southern Ethiopia. Geocarto International. 38(1):2229952. doi: 10.1080/10106049.2023.2229952.

Abro TW, Debie E. 2024. Soil erosion assessment for prioritizing soil and water conservation interventions in Gotu watershed, Northeastern Ethiopia. Environ Monit Assess. 196(11): 1149. doi: 10.1007/s10661-024-13338-y.

Hammad AbuLundekvam H, Børresen T. 2004. Adaptation of RUSLE in the eastern part of the Mediterranean region. Environ Manage. 34(6):829–841. 10.1007/s00267-003-0296-7

Agegnehu N, Naqvi HR, Alemayehu D. 2022. Rainfall induced soil erosion assessment, prioritization and conservation treatment using RUSLE and SYI models in highland watershed of Ethiopia. Geocarto International. 37(9):2524–2540. doi: 10.1080/10106049.2020.1822927.

Ahmed J S, Buizza R, Dell'Acqua M, Demissie T, Pe M E. 2024. Evaluation of ERA5 and CHIRPS rainfall estimates against observations across Ethiopia. Meteorol. Atmos. Phys. 136(3):17–17-. 10.1007/s00703-024-01008-0.

Alam A, Sultan BM, Maheen M. 2020. Using Landsat satellite data for assessing the land use and land cover change in Kashmir valley. Geo. Journal. 85(6):1529–1543. doi: 10.1007/s10708-019-10037-x.

Alexandridis TK, Sotiropoulou AM, Bilas G, Karapetsas N, Silleos NG. 2015. The efects of seasonality in estimating the C-factor of soil Erosion studies. Land Degrad Dev. 26(6):596–603. doi: 10.1002/ldr.2223.

Alhamshry A, Fenta A, Yasuda H, Kimura R, Shimizu K. 2019. Seasonal rainfall variability in Ethiopia and its long-term link to global sea surface temperatures. Water. 12(1):55. doi: 10.3390/w12010055.

Amsalu T, Mengaw A. 2014. GIS based soil loss estimation using rusle model: the case of jabi tehinan woreda, ANRS, Ethiopia. Nat. Resour. 5(11):11–11-. doi 10.4236/nr.2014.511054.

Aneseyee AB, Elias E, Soromessa T, Feyisa GL. 2020. Land use/land cover change effect on soil erosion and sediment delivery in the Winike watershed, Omo Gibe Basin Ethiopia. Sci Total Environ. 728:138776. doi: 10.1016/j.scitotenv.2020.138776.

Balabathina V, Raju R P, Mulualem W. 2019. Integrated remote sensing and GIS-based universal soil loss equation for soil erosion estimation in the Megech River Catchment, Tana Lake Sub-basin, Northwestern Ethiopia. Am J Geogr Inf Syst. 8(4):141–157. DOI: 10.5923/j.ajgis.20190804.01.

Barakat A, Khellouk R, Jazouli A, Touhami F, Nadem S. 2018. Monitoring of forest cover dynamics in eastern area of Béni-Mellal Province using ASTER and Sentinel-2A multispectral data. Geol Ecol Landscapes. 2(3):203–215. doi: 10.1080/24749508.2018.1452478.

Bekele B, Gemi Y. 2021. Soil erosion risk and sediment yield assessment with universal soil loss equation and GIS: in Dijo watershed, Rift valley Basin of Ethiopia. Model Earth Syst Environ. 7(1):273–291. doi: 10.1007/s40808-020-01017-z.

Belay B, Mengistu DA. 2021. Impacts of land use/land cover and climate changes on soil erosion in Muga watershed, Upper Blue Nile basin (Abay), Ethiopia. Ecol Process. 10(1):68. doi: 10.1186/s13717-021-00339-9.

Belayneh M, Yirgu T, Tsegaye D. 2019. Potential soil erosion estimation and area prioritization for better conservation planning in Gumara watershed using RUSLE and GIS techniques. Environ Syst Res. 8(1):20. doi: 10.1186/s40068-019-0149-x.

Berberoglu S, Cilek A, Kirkby M, Irvine B, Donmez C. 2020. Spatial and temporal evaluation of soil erosion in Turkey under climate change scenarios using the Pan-European Soil Erosion Risk Assessment (PESERA) model. Environ Monit Assess. 192(8):491. doi: 10.1007/s10661-020-08429-5.

Berihun ML, Tsunekawa A, Haregeweyn N, Meshesha DT, Adgo E, Tsubo M, Masunaga T, Fenta AA, Sultan D, Yibeltal M, et al. 2019. Hydrological responses to land use/land cover change and climate variability in contrasting agro-ecological environments of the Upper Blue Nile basin, Ethiopia. Sci Total Environ. 689:347–365. doi: 10.1016/j.scito.tenv.2019.06.338

Besha KZ, Demissie TA, Feyessa FF. 2024. Effects of land use/land cover change on hydrological responses of a watershed in the Central Rift Valley of Ethiopia. Hydrology Research. 55(2):83–111. doi: 10.2166/nh.2024.042.

Borrelli P, Robinson DA, Panagos P, Lugato E, Yang JE, Alewell C, Wuepper D, Montanarella L, Ballabio C. 2020. Land use and climate change impacts on global soil erosion by water (2015–2070). Proc Natl Acad Sci 117(36):p. 21994–22001. doi: 10.1073/pnas.2001403117.

Chakrabortty R, Pradhan B, Mondal P, Pal SC. 2020b. The use of RUSLE and GCMs to predict potential soil erosion associated with climate change in a monsoon dominated region of eastern India. Arab J Geosci. 13(20):1–20. doi: 10.1007/s12517-020-06033-y.

Chalise D, Kumar L, Kristiansen P. 2019. Land degradation by soil erosion in Nepal: a review. Soil Systems. 3(1):12. doi: 10.3390/soilsystems3010012.

Chavez PS. 1988. An improved dark-object subtraction technique for atmospheric scattering correction of multispectral data. Remote Sens. Environ. 24(3):459–479. 10.1016/0034-4257(88)90019-3.

Chen L, Guo Z, Yin K, Shrestha D, Jin s 2019. The influence of land use and land cover change on landslide susceptibility: a case study in Zhushan Town, Xuan'en County (Hubei, China). Nat Hazards Earth Syst Sci. 19(10):2207–2228. doi: 10.5194/nhess-19-2207-2019.

Ciampalini R, Constantine JA, Walker-Springett KJ, Hales TC, Ormerod SJ, Hall IR. 2020. Modelling soil erosion responses to climate change in three catchments of Great Britain. Sci Total Environ. 749:141657. doi: 10.1016/j.scitotenv.2020.141657.

Currit N. 2005. Development of a remotely sensed, historical land-cover change database for rural Chihuahua, Mexico. Int J Appl Earth Obs Geoinf. 7(3):232–247. doi: 10.1016/j.jag.2005.05.001.

Degife A, Worku H, Gizaw S. 2021. Environmental implications of soil erosion and sediment yield in Lake Hawassa watershed, south-central Ethiopia. Environ Syst Res. 10(28):1–24. 10.1186/s40068-021-00232-6.

Desalegn A, Tezera A, Tesfay F. 2018. Developing GIS-based soil erosion map using RUSLE of Andit Tid Watershed, central highlands of Ethiopia. JSRR. 19(1):1–13. doi: 10.9734/JSRR/2018/40841.

Du H, Tan ML, Zhang Fei, Chun KP, Li L, Kabir MH. 2024. Evaluating the effectiveness of CHIRPS data for hydroclimatic studies. Theor Appl Climatol. 155(3):1519–1539. 10.1007/s00704-023-04721-9.

Duarte L, Cunha M, Teodoro AC. 2021. Comparing hydric erosion soil loss models in rainy mountainous and dry flat regions in Portugal. Land. 10(6):554. doi: 10.3390/land10060554.

Ebabu K, Tsunekawa A, Haregeweyn N, Adgo E, Meshesha DT, Aklog D, Masunaga T, Tsubo M, Sultan D, Fenta AA, et al. 2019. Efects of land use and sustainable land management practices on runof and soil loss in the Upper Blue Nile basin, Ethiopia. Sci Total Environ. 648:1462–1475. doi: 10.1016/j.scitotenv.2018.08.273.

Eekhout JP, De Vente J. 2020. How soil erosion model conceptualization afects soil loss projections under climate change. Progr Phys Geogr Earth Env. 44(2):212–232. 10.1177/0309133319871937

Eleni Y, Wolfgang W, Michael E, Dagnachew L, Günter B. 2013. Identifying land use/cover dynamics in the Koga Catchment, Ethiopia, from multi-scale data, and implications for environmental change. ISPRS Inter J Geo-Info. 2:302–323.

Farhan Y, Zregat D, Farhan I. 2013. Spatial estimation of soil erosion risk using RUSLE approach, RS, and GIS techniques: a case study of Kufranja watershed, Northern Jordan. JWARP. 05(12):1247–1261. doi: 10.4236/jwarp.2013.512134.

Fazzini M, Bisci C, Billi P. 2015. The climate of Ethiopia. In: Billi P, editor. Landscapes and landforms of Ethiopia. World geomorphologic landscapes.Dordrecht: Springer.

Fu BJ, Zhao WW, Chen LD, Zhang QJ, Lü YH, Gulinck H, Poesen J. 2005. Assessment of soil erosion at large watershed scale using RUSLE and GIS: a case study in the Loess Plateau of China. Land Degrad Dev. 16(1):73–85. doi: 10.1002/ldr.646.

Funk C, Peterson P, Landsfeld M, Pedreros D, Verdin J, Shukla S, Husak G, Rowland J, Harrison L, Hoell A, et al. 2015. The climate hazards infrared precipitation with stations – a new environmental record for monitoring extremes. Sci Data. 2(1):150066. doi: 10.1038/sdata.2015.66.

Ganasri BP, Ramesh H. 2016. Assessment of soil erosion by RUSLE model using remote sensing and GIS – a case study of Nethravathi Basin. Geosci Front. 7(6):953–961. doi: 10.1016/j.gsf.2015.10.007.

Gashaw T, Tulu T, Argaw M, Worqlul AW. 2019. Modeling the impacts of land use–land cover changes on soil erosion and sediment yield in the Andassa watershed, upper Blue Nile basin. Environ Earth Sci. 78(24):679. doi: 10.1007/s12665-019-8726-x.

Gelagay HS, Minale AS. 2016. Soil loss estimation using GIS and Remote sensing techniques: a case of Koga watershed, Northwestern Ethiopia. Int Soil Water Conservat Res. 4(2):126–136. doi: 10.1016/j.iswcr.2016.01.002.

Gessesse B, Bewket W, Bräuning A. 2015. Model-based characterization and monitoring of run of and soil erosion in response to land use/land cover changes in the Modjo watershed, Ethiopia. Land Degrad Dev. 26(7):711–724. doi: 10.1002/ldr.2276.

Girmay G, Moges A, Muluneh A. 2020. Estimation of soil loss rate using the USLE model for Agewmariayam Watershed, northern Ethiopia. Agric Food Secur. 9(1):9. doi: 10.1186/s40066-020-00262-w.

Girmay G, Moges A, Muluneh A. 2021. Assessment of current and future climate change impact on soil loss rate of Agewmariam Watershed, Northern Ethiopia. Air Soil Water Res. 14:1178622121995847. https://uk.sagepub.com/en-gb/journals-permissions. doi: 10.1177/1178622121995847.

Greenland DJ. 2001. Soil fertility management in support of food security in sub-Saharan Africa. Rome: Food and Agriculture Organization of the United Nation.

Gurmu Z, Ritzema H, Fraiture C, Riksen M, Ayana M. 2021. Sediment influx and its drivers in farmers' managed irrigation schemes in Ethiopia. Water. 13(13):1747. doi: 10.3390/w13131747.

Haregeweyn N, Tsunekawa A, Poesen J, Tsubo M, Meshesha DT, Fenta AA, Nyssen J, Adgo E. 2017. Comprehensive assessment of soil erosion risk for better land use planning in river

basins: case study of Upper Blue Nile River. Sci Total Environ. 574:95–108. doi: 10.1016/j.scito.tenv.2016.09.019
Heyder SM, Beza SA, Demissie ST. 2023. Optimization of land management measures for soil erosion risk using GIS in agricultural landscape of western Hararghe highlands. Ethiopia. Scientif African. 21:e01853. doi: 10.1016/j.geodrs.2018.01.002.
Huang C, Zhou Z, Teng M, Wu C, Wang P. 2020. Effects of climate, land use and land cover changes on soil loss in the Three Gorges Reservoir area, China. Geograp Sustainabil. 1(3): 200–208. doi: 10.1016/j.geosus.2020.08.001.
Huang F, Chen J, Yao C, Chang Z, Jiang Q, Li S, Guo S. 2020. SUSLE: a slope and seasonal rainfall-based RUSLE model for regional quantitative prediction of soil erosion. Bull Eng Geol Environ. 79(10):5213–5228. doi: 10.1007/s10064-020-01886-9.
Hurni H. 1985. Erosion–productivity–conservation systems in Ethiopia. Paper presented at the 4th international conference on soil conservation, Maracacy, Venezuela, 3–9 November 1985.
Hurni H, Berhanu D, Gete Z. 2015a. Saving Ethiopia's soils. In: Ehrensperger A, Ott C, Wiesmann U, editor. Eastern and Southern Africa Partnership Programme: highlights from 15 years of joint action for sustainable development. Centre for Development and Environment. Bern: University of Bern with Bern Open Publishing, p. 27–30. doi: 10.7892/boris.72023.
Hurni K, Zeleke G, Kassie M, Tegegne B, Kassawmar T, Teferi E, Moges A, Tadesse D, Ahmed M, Degu Y, et al. 2015b. Soil degradation and sustainable land management in the rainfed agricultural areas of Ethiopia: an assessment of the economic implications. Report for the economics of land degradation initiative.
Hurni K, Zeleke G, Kassie M, Tegegne B, Kassawmar T, Teferi E, Moges A, Tadesse D, Ahmed M, Degu Y. 2015. Soil degradation and sustainable land management in the rainfed agricultural areas of Ethiopia: an assessment of the economic implications. Report for the Economics of Land Degradation Initiative.
Kavian A, Hoseinpoor SS, Solaimani K, Jafari B. 2017. Simulating the effects of land-use changes on soil erosion using the RUSLE model. Geocarto Int. 32(1):97–111. doi: 10.1080/10106049.2015.1130083.
Keesstra S, Mol G, De Leeuw J, Okx J, Molenaar C, De Cleen M, Visser S. 2018. Soil-related sustainable development goals: four concepts to make land degradation neutrality and restoration work. Land. 7(4):133. doi: 10.3390/land7040133.
Kidane M, Bezie A, Kesete N, Tolessa T. 2019. The impact of land use and land cover (LULC) dynamics on soil erosion and sediment yield in Ethiopia. Heliyon. 5(12):e0298. doi: 10.1016/j.heliyon.2019.e02981.
Kulimushi LC, Choudhari P, Maniragaba A, Elbeltagi A, Mugabowindekwe M, Rwanyiziri G, Byizigiro RV, Pingale SM, Singh SK. 2021. Erosion risk assessment through prioritization of sub-watersheds in Nyabarongo river catchment, Rwanda. Environm Chall. 5:100260. doi: 10.1016/j.envc.2021.100260.
Kulimushi LC, Maniragaba A, Choudhari P, Elbeltagi A, Uwemeye J, Rushema E, Singh SK. 2021. Evaluation of soil erosion and sediment yield spatio-temporal pattern during 1990–2019. Geomatics Nat Hazards Risk. 12(1):2676–2707. doi: 10.1080/19475705.2021.1973118.
Kumar N, Singh SK. 2021. Soil erosion assessment using earth observation data in a transboundary river basin. Nat Hazards. 107(1):1–34. doi: 10.1007/s11069-021-04571-6.
Lanorte A, Cillis G, Calamita G, Nolè G, Pilogallo A, Tucci B, De Santis F. 2019. Integrated approach of RUSLE, GIS and ESA sentinel-2 satellite data for post-fire soil erosion assessment in Basilicata Region (Southern Italy). Geomat. Nat. Hazards Risk. 10(1):1563–1595. doi: 10.1080/19475705.2019.1578271.
Lee S. 2004. Soil erosion assessment and its verification using the Universal Soil Loss Equation and Geographic Information System: a case study at Boun, Korea. Environ. Geol. 45(4):457–465. 10.1007/s00254-003-0897-8.

Li F, Jupp DLB, Reddy S, Lymburner Leo, Mueller N, Tan P, Islam A. 2010. An Evaluation of the Use of Atmospheric and BRDF Correction to Standardize Landsat Data. IEEE J Sel Top Appl Earth Observations Remote Sensing. 3(3):257–270. 10.1109/JSTARS.2010.2042281.

Li C, Li Z, Yang M, Ma B, Wang B. 2021. Grid-scale impact of climate change and human influence on soil erosion within East African Highlands (Kagera Basin). IJERPH. 18(5):2775. doi: 10.3390/ijerph18052775.

Li M, Zang S, Zhang B, Li S, Wu C. 2014. A review of remote sensing image classification techniques: the role of spatio-contextual information. Europ J Remote Sens. 47(1):389–411. doi: 10.5721/EuJRS20144723.

Luetzenburg G, Bittner MJ, Calsamiglia A, Renschler CS, Estrany J, Poeppl R. 2020. Climate and land use change effects on soil erosion in two small agricultural catchment systems Fugnitz–Austria. Can Revull–Spain. Sci Total Environ. 704:135389. doi: 10.1016/j.scitotenv.2019.135389.

Maliqi E, Singh SK. 2019. Quantitative estimation of soil erosion using open-access earth observation data sets and erosion potential model. Water Conserv Sci Eng. 4(4):187–200. doi: 10.1007/s41101-019-00078-1.

Markose VJ, Jayappa KS. 2016. Soil loss estimation and prioritization of sub-watersheds of Kali River basin, Karnataka, India, using RUSLE and GIS. Environ Monit Assess. 188(4):225. doi: 10.1007/s10661-016-5218-2.

Mitasova H, Mitas Z. 1999. Modeling soil detachment with RUSLE 3D using GIS. Champaign: University of Illinois at Urbana Champaign.

Moges DM, Bhat HG. 2017. Integration of geospatial technologies with RUSLE for analysis of land use/cover change impact on soil erosion: case study in Rib watershed, north-western highland Ethiopia. Environ Earth Sci. 76(22):765. doi: 10.1007/s12665-017-7109-4.

Mohajane M, Essahlaoui A, Oudija F, Hafyani M, Hmaidi A, Ouali A, Randazzo G, Teodoro A. 2018. Land Use/Land Cover (LULC) Using Landsat Data Series (MSS, TM, ETM+ and OLI) in Azrou Forest, in the Central Middle Atlas of Morocco. Environments. 5(12):131. (doi: 10.3390/environments5120131.

Negese A. 2021. Impacts of land use and land cover change on soil erosion and hydrological responses in Ethiopia. Appl Environ Soil Sci. 2021:1–10. doi: 10.1155/2021/6669438.

Nigussie W, Hailu BT, Azagegn T. 2019. Mapping of groundwater potential zones using sentinel satellites (−1 SAR and -2A MSI) images and analytical hierarchy process in Ketar watershed, Main Ethiopian Rift. J Afr Earth Sci. 160:103632. doi: 10.1016/j.jafrearsci.2019.103632.

Nyssen J, Clymans W, Poesen J, Vandecasteele I, De Baets S, Haregeweyn N, Naudts J, Hadera A, Moeyersons J, Haile M, et al. 2009. How soil conservation affects the catchment sediment budget: a comprehensive study in the North Ethiopian highlands. Earth Surf Processes Landf. 34(9):1216–1233. doi: 10.1002/esp.1805.

Nyssen Jan, Poesen J, Moeyersons Jan, Deckers J, Haile M, Lang A. 2004. Human impact on the environment in the Ethiopian and Eritrean highlands—a state of the art. Earth Sci. Rev. 64(3-4):273–320. 10.1016/S0012-8252(03)00078-3.

Nyssen J, Poesen J, Moeyersons J, Haile M, Deckers J. 2008. Dynamics of soil erosion rates and controlling factors in the Northern Ethiopian Highlands – towards a sediment budget. Earth Surf Processes Landf. 33(5):695–711. doi: 10.1002/esp.1569.

Osunmadewa BA, Gebrehiwot WZ, Csaplovics E, Adeofun OC. 2018. Spatio-temporal monitoring of vegetation phenology in the dry sub-humid region of Nigeria using time series of AVHRR NDVI and TAMSAT datasets. Open Geosci. 10(1):1–11. doi: 10.1515/geo-2018-0001.

Ozsahin E, Duru U, Eroglu I. 2018. Land use and land cover changes (LULCC), a key to understand soil erosion intensities in the Maritsa Basin. Water. 10(3):335. doi: 10.3390/w10030335.

Pal M, Mather PM. 2003. An assessment of the effectiveness of decision tree methods for land cover classification. Remote Sens. Environ. 86(4):554–565. doi: 10.1016/S0034-4257(03)00132-9.

Pal SC, Chakrabortty R. 2019. Simulating the impact of climate change on soil erosion in sub-tropical monsoon dominated watershed based on RUSLE, SCS runoff and MIROC5 climatic model. Adv Space Res. 64(2):352–377. doi: 10.1016/j.asr.2019.04.033.

Pal SC, Chakrabortty R, Roy P, Chowdhuri C, Das B, Saha A, Shit M. 2021. Changing climate and land use of 21st century influences soil erosion in India. Gondwana Res. 94:164–185. doi: 10.1016/j.gr.2021.02.021.

Paredes-Trejo F, Barbosa HA, Kumar TVL, Thakur MK, Buriti CO. 2020. Assessment of the CHIRPS-Based Satellite Precipitation Estimates. Inland Waters - Dynamics and Ecology. doi: 10.5772/intechopen.91472. Available from: https://www.intechopen.com/chapters/71449.

Phinzi K, Ngetar NS. 2019. Land use/land cover dynamics and soil erosion in the Umzintlava catchment (T32E), Eastern Cape, South Africa. Trans R Soc South Africa. 74(3):223–237. doi: 10.1080/0035919X.2019.1634652.

Rawat KS, Singh SK. 2018. Appraisal of soil conservation capacity using NDVI model-based C factor of RUSLE model for a semi-arid ungauged watershed: a case study. Water Conserv Sci Eng. 3(1):47–58. doi: 10.1007/s41101-018-0042-x.

Reda D, Engida N, Asfaw H, Hamdi R. 2015. Analysis of precipitation based on ensembles of regional climate model simulations and observational databases over Ethiopia for the period 1989–2008. Intl J Climatol. 35(6):948–971. doi: 10.1002/joc.4029.

Renard KG, Foster GR, Weeies GA, McCool DK, Yoder DC. 1997. Predicting soil erosion by water: a guide to conservation planning with the Revised Universal Soil Loss Equation (RUSLE). USDA Agriculture Handbook No. 703, Washington, DC.

Rust N, Lunder OE, Iversen S, Vella S, Oughton EA, Breland TA, Glass JH, Maynard CM, McMorran R, Reed MS. 2022. Perceived causes and solutions to soil degradation in the UK and Norway. Land. 11(1):131. doi: 10.3390/land11010131.

Samela C, Imbrenda V, Coluzzi R, Pace L, Simoniello T, Lanfredi M. 2022. Multi-decadal assessment of soil loss in a mediterranean region characterized by contrasting local climates. Land. 11(7):1010. doi: 10.3390/land11071010.

Sharma A, Tiwari KN, Bhadoria PBS. 2011. Effect of land use land cover change on soil erosion potential in an agricultural watershed. Environ Monit Assess. 173(1–4):789–801. doi: 10.1007/s10661-010-1423-6.

Sharma DIJ, Prasad R, Mishra PVN, Yadav VP, Bala R. 2018. Land use and Land cover classification of multispectral landsat-8 satellite imagery using discrete wavelet transform. The International Archives of the Photogrammetry, Remote Sensing and Spatial Information Sciences, XLII-5, 2018 ISPRS TC V Mid-term Symposium "Geospatial Technology – Pixel to People, 20–23 November 2018.

Sidi Almouctar MA, Wu Y, Zhao F, Dossou JF. 2021. Soil Erosion Assessment Using the RUSLE Model and Geospatial Techniques (Remote Sensing and GIS) in South-Central Niger (Maradi Region). Water. 13(24):3511. doi: 10.3390/w13243511.

Sime C, Demissie T, Tufa F. 2020. Surface runoff modeling in Ketar watershed, Ethiopia. J Sediment Environ. 5(1):151–162. doi: 10.1007/s43217-020-00009-4.

Simms AD, Woodrofe CD, Jones BG. 2003. Application of RUSLE for erosion management in a coastal catchment, Southern NSW. In Proceedings of the International Congress on Modeling and Simulation: integrative

Singh R. 2023. Impact of climate and land use land cover changes on soil erosion. In Soil and Water Conservation Structures Design. Water Science and Technology Library, 123. Singapore: Springer. doi: 10.1007/978-981-19-8665-9_14.

Sotiropoulou AM, Alexandridis T, Bilas G, Karapetsas N, Tzellou A, Silleos N, Misopolinos N. 2011. A user friendly GIS model for the estimation of erosion risk in agricultural land using the USLE. In Proceedings of the International Conference on Information and Communication Technologies for Sustainable Agri-production and Environment, 8–11 September, 2011, 795– 801, 2011.

Tadesse L, Suryabhagavan KV, Sridhar G, Legesse G. 2017. Land use and land cover changes and Soil erosion in Yezat Watershed, North Western Ethiopia. Int Soil Water Conserv Res. 5(2):85–94. doi: 10.1016/j.iswcr.2017.05.004.

Taye G, Vanmaercke M, Poesen J, Van Wesemael B, Tesfaye S, Teka D, Nyssen J, Deckers J, Haregeweyn N. 2018. Determining RUSLE P- and C-factors for stone bunds and trenches in rangeland and cropland North Ethiopia. Land Degrad Dev. 29(3):812–824. doi: 10.1002/ldr.2814.

Tesfamariam B, Gessesse B, Melgan F. 2022. MaxEnt-based modeling of suitable habitat for rehabilitation of Podocarpus forest at landscape-scale. Environ Syst Res. 11(1):4. doi: 10.1186/s40068-022-00248-6.

Tsai F, Lai JS, Nguyen KA, Chen W. 2021. Determining cover management factor with remote sensing and spatial analysis for improving long-term soil loss estimation in watersheds. IJGI. 10(1):19. doi: 10.3390/ijgi10010019.

Ullah S, Khan M, Qiao X. 2024. Examining the impact of land use and land cover changes on land surface temperature in Herat city using machine learning algorithms. GeoJournal. 89(5):225. doi: 10.1007/s10708-024-11217-0.

Ullah S, Qiao X, Tariq A. 2025. Impact assessment of planned and unplanned urbanization on land surface temperature in Afghanistan using machine learning algorithms: a path toward sustainability. Sci Rep. 15(1):3092. doi: 10.1038/s41598-025-87234-x.

Ullah W, Ahmad K, Tahir AA, Ullah S, Rafiq MT, Abdullah-Al-Wadud M. 2025. Impacts of tourism on LULC and LST dynamics in district Buner and Shangla, Pakistan. Sci Rep. 15(1):9304. doi: 10.1038/s41598-025-94230-8.

Vianney Nsabiyumva JM, Apollonio C, Castelli G, Petroselli A, Sabir M, Preti F. 2023. Agricultural practices for hillslope erosion mitigation: a case study in Morocco. Water. 15(11):2120. doi: 10.3390/w15112120.

Wang G, Gertner G, Singh V, Shinkareva S, Parysow P, Anderson A. 2002. Spatial and temporal prediction and uncertainty of soil loss using the revised universal soil loss equation: A case study of the rainfall-runoff erosivity R factor. Ecol. Model. 153(1-2):143–155. doi: 10.1016/S0304-3800(01)00507-5.

Wang S, Sun B, Li C, Li Z, Ma B. 2018. Runoff and soil erosion on Slope Cropland: A review. J Resour Ecol. 9:461–470.

Wang Y, Cheng C, Xie Y, Liu B, Yin S, Liu Y, Hao Y. 2017. Increasing trends in rainfall-runoff erosivity in the Source Region of the Three Rivers, 1961–2012. Sci Total Environ. 592:639–648. doi: 10.1016/j.scitotenv.2017.02.235.

Wijitkosum S. 2012. Impacts of land use changes on soil erosion in Pa Deng sub-district, adjacent area of Kaeng Krachan National Park, Thailand. Soil Water Res. 7(1):10–17.

Wischmeier WH, Smith DD. 1978. Predicting rainfall-erosion losses – a guide to conservation planning. USDA Agriculture Handbook No. 537. Washington, DC.

Xavier APC, Silva RM, Silva AM, Santos CAG. 2016. Mapping soil erosion vulnerability using remote sensing and GIS: a case study of Mamuaba watershed. Revista Brasileira de Cartografi a, Rio De Janeiro. 68(9):1677–1688.

Zerihun M, Mohammedyasin MS, Sewnet D, Adem AA, Lakew M. 2018. Assessment of soil erosion using RUSLE, GIS and remote sensing in NW Ethiopia. Geoderma Regional. 12:83–90. doi: 10.1016/j.geodrs.2018.01.002.

Zhang A, Tariq A, Quddoos A, Naz I, Aslam RW, Barboza E, Ullah S, Abdullah-Al-Wadud M. 2025. Spatio-temporal analysis of urban expansion and land use dynamics using google earth engine and predictive models. Sci Rep. 15(1):6993. doi: 10.1038/s41598-025-92034-4.